Functional Connectivity Analysis on Resting State Electroencephalography Signals Following Chiropractic Spinal Manipulation in Chronic Stroke Patients

Toby Steven Waterstone
Biomedical Engineering & Informatics
4^{th} Semester

Master's Thesis
Department of Health Science & Technology

Spring 2019

AALBORG UNIVERSITY
DENMARK

CENTRE FOR CHIROPRACTIC RESEARCH
New Zealand College of Chiropractic

4rd Semester, Master's Thesis

School of Medicine and Health

Biomedical Engineering & Informatics

Fredrik Bajers Vej 7A, 9220 Aalborg

Title: Functional Connectivity Analysis on Resting State Electroencephalography Signals Following Chiropractic Spinal Manipulation in Chronic Stroke Patients

Theme:
Master's thesis

Project period:
Spring 2019
1st February 2019 - 6th June 2019

Project group:
19gr10404

Participants:
Toby Steven Waterstone

Supervisors:
Afshin Samani
Imran Khan Niazi

Pages: 62
Appendix: 9
Handed in: 06/06/2019

Abstract

Background Stroke is a global problem affecting billions of people. Many of these patients suffers from post stroke impairments, which can both be present as cognitive and motor deficits, which results in a decline in life quality. Early and effective rehabilitation are therefore important for these patients, as recovery and mechanisms, like neuroplasticity, linked to recovery are maximized at the early stages of stroke.
Methods The present study investigated chiropractic spinal manipulation (SM) and its effects on resting state functional connectivity in chronic stroke patients. Functional connectivity analysis were computed through the metrics of Mutual Information (MI) and Phase Lag Index (PLI). Non-parametric cluster based permutation test were used to asses the statistical significance of the dataset within both SM session and a control session and between the two, in order to evaluate the effect of the interventions.
Results Significantly increased functional connectivity of PLI were found within the Default Mode Network (DMN), between the posterior cingulate cortex and parahippocampal regions, for the SM session. No significant changes occurred for the control session or for the MI metric.
Conclusion These findings suggests that SM alters functional connectivity in the brain of chronic stroke patients. The patients might have experienced a decreased pain perception, episodic memory and spatial representation and navigation. But it is uncertain, as these effects were not included in the study. Therefore further research regarding the effects of these results and SM, taking into account further information, are needed in order to validate if stroke patients can benefit from SM in a rehabilitation program.

Preface

This master's thesis was carried out by group 19gr10404 in Biomedical Engineering & informatics, at Aalborg University, written in the period from February 1st 2019 to June 6th 2019. The study were purposed and carried out in collaboration with the New Zealand College of Chiropractic (NZCC) research department.

Readers guide

The Harvard method was used in cite relevant references from the literature. Surname of the author long with year of publication are cited in squared brackets as following, [surname, year]. the complete reference list are listed at the end of the report, previous to the appendix. References are listed in alphabetic and numbered.

References to tables and figures are expressed by their corresponding number, which are indicated according to their order, in the respective section. For instance, a table that are the ninth in fourth chapter are numbered Table 4.9. Tables descriptions are located at the top of the belonging table, while figure descriptions are located at the bottom of the belonging figure.

Abbreviations are initially written out when presented, with the abbreviation in parentheses. Afterwards the abbreviation will only be stated.

Acknowledgments

I would like to thank my supervisors Afshin Samani and Imran Khan Niazi for excellent supervision during the project period.

Toby Steven Waterstone

<twater14@student.aau.dk>

Content

1 | Introduction

Stroke is a health care problem that affects millions of people world wide and it is the number one cause of chronic disability in patients [Brody et al. (2014)]. the prevalence of stroke is estimated to be 9.6 million people in Europe and the third most likely cause of death in industrialized countries, killing approximately 5.7 million people world wide each year [Hennerici et al. (2012)]. Stroke also accounts for a big part of the economical and occupational burden within the health care sector, as it is estimated that 2 to 3% of all health care services are contributed by stroke, in Europe. In 2006 the cost were estimated €38 billion. Even though stroke accounts for a lot health care services, it is estimated that only 40% of stroke survivors gets the optimal treatment in order to get full recovery and in gaining independence post stroke. The disabilities that stoke survivors experience are often long lasting and can be present as both impaired cognitive and motor function [Hennerici et al. (2012)]. Rehabilitation of stroke patients are of great importance, especially in the early stages after the acute phase, as mechanisms like neuoplasticity plays a big part of the recovery, where the brain reorganizes and adapts to the lesion which the stoke have caused [Mir et al. (2014), Endres et al. (2008)]. Rehabilitation methods which take these properties into account are therefore effective in getting a successful recovery of the patients [Endres et al. (2008)] During the past decades a growing body of research concerning chiropractic spinal manipulation (SM) in relation to its effects on the central nervous system (CNS), has been established [Haavik & Murphy (2012), Haavik (2014), Niazi et al. (2015), Christiansen et al. (2018)]. The chiropractic profession considers the relationship between the spine and nervous system. Research suggests that SM alters the way the brain processes information related to afferent input [Haavik & Murphy (2012)]. Some of the previous studies that interests SM have done research on several aspects of the nervous system, like motor output, sensory processing, functional performance and sensorimotor integration [Johnson (2013)]. These studies all contribute to the hypothesized model, described by Haavik & Murphy (2012), which gives detail about the mechanisms of chiropractic on an scientific level and how SM alters the bodies function, by inducing optimal function of the CNS [Haavik & Murphy (2012)].
A recent study by Holt et al. (2019) demonstrated that SM altered neural threshold related to neural mechanisms, along with an increased force production of planter flexor muscle, in chronic stroke patients. Although there are evidence on the mechanisms behind some of the effects following SM, the mechanisms that concerns CNS and more specifically the changes that happens in the cortex level has only scarcely been investigated. One study by Gay et al. (2014) investigated the effect of manual therapy, including SM, and found alterations within the functional connectivity of brain regions along with a decrease in pain perception. The aim of this study is therefore to explore the effects of SM in chronic stroke patients, in order to see if neurophysiological changes are present following single session SM, by performing functional connectivity analysis on electroencephalography (EEG) signals in these patients, in order to review the relevance of chiropractic SM in a rehabilitation program.

2 | Background

2.1 Stroke

In this section, the definition of stroke and its mechanisms are presented. Initially, before the definition of stroke is explained, the anatomy of the brain is outlined, in order to better understand the mechanisms of stroke and how it emerges.

2.1.1 Anatomy of the brain

The brain is an important organ, as it is the organ responsible for many vital functions of the human body. It is comprised of billions of neurons with high demands for oxygen and nutrients from the blood circulatory system. In order to understand how stroke emerges and affects the brain, the brain and circulatory system that supplies the brain with oxygenated blood is important to understand, as stroke can have very different symptoms when patients experience a stroke, depending on the type and location in the circulatory system a stroke emerges [Mir et al. (2014)]. The brain can be divided into lobes as regions that are responsible for different functions in the body. Figure figure 2.1 shows how the brain is divided into regions [et. al. Martini (2012)].

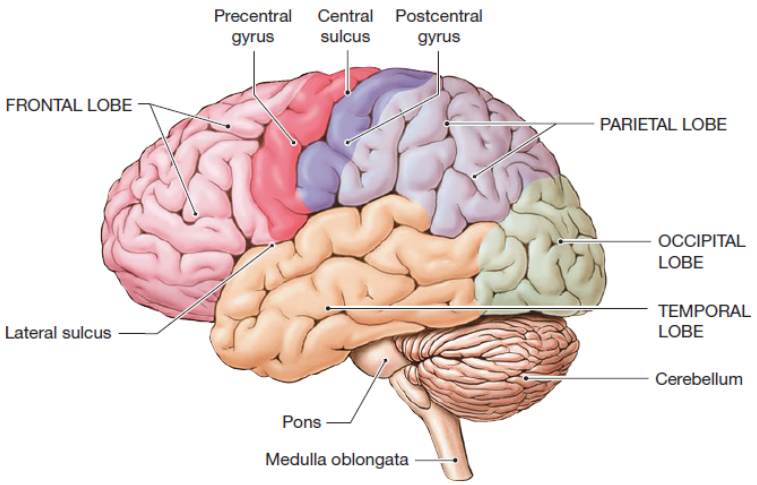

Figure 2.1: Location of the different regions of the brain, lateral view [et. al. Martini (2012)].

The brain, or more specifically the cerebrum is divided into four lobes, the frontal lobe, the parietal lobe, the temporal lobe and the occipital lobe. The frontal lobe contains regions responsible for cognitive tasks such as concentration, planning and problem solving, voluntary movement and speech. The parietal lobe contains regions responsible for sensory input and body awareness. The temporal lobe contains regions responsible for hearing, language, emotions and long term memory. The occipital lobe contains regions

responsible for vision. Finally the cerebellum is responsible for fine motor control, balance and coordination [et. al. Martini (2012)]. From this knowledge the location of a stroke can be related to functions corresponding to specific parts of the brain and will be expressed by decreased activity of these functions [Hennerici et al. (2012)]. Symptoms can range from sudden weakness or numb extremities, such as difficulties controlling the arms, legs or face muscles. Speech or language understanding problems, vision decrease, headache, dizziness and loss of balance are also common symptoms [Mayfield (2019)].

Figure figure 2.2 shows the organization of the arteries that supplies the different regions of the brain with blood.

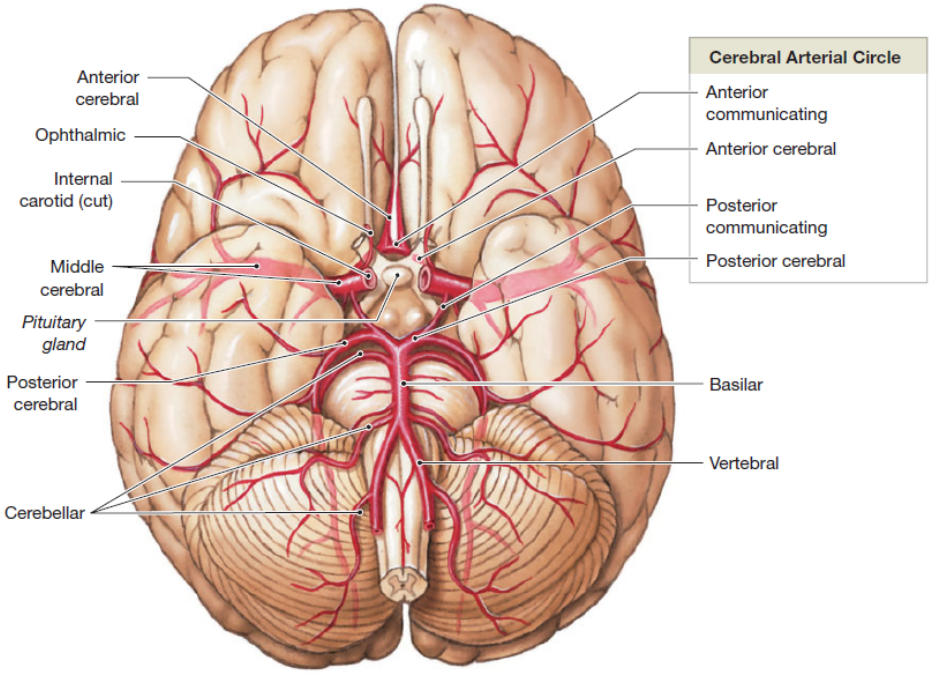

Figure 2.2: Blood circulatory system of the brain arteries, inferior view [et. al. Martini (2012)].

The blood supply to the brain is delivered by two paired arteries originating close to the aorta. These arteries are the internal carotid originating from the common carotid arteries, and the ventral arteries, which merge into the basilar arteries. In the brain these arteries communicate through the so called Circle of Willis, which branches out to smaller arteries that goes to different regions of the brain. The internal carotid arteries mainly supply the anterior and middle regions of the brain. It is responsible for supplying the eyes through the ophthalmic artery, the frontal and parietal lobes through the anterior cerebral artery, the midbrain and cerebral hemisphere lateral surface through the middle cerebral artery. The ventral arteries mainly supply the posterior regions of the brain. These include the spinal cord, pons, medulla oblongata, the occipital lobe and cerebellum [et. al. Martini (2012)].

2.1.2 Definition of stroke

Stroke is characterized by abrupt loss of brain function caused by interference of the blood supply to the central nervous system. An amount of 50 - 60 ml/100g/min is the normal volume of blood, which flows through the brain. If this flow decreases to under 10 ml/100g/min it results in ischemia and therefore damage to the brains tissue, which lack the blood flow, caused by starvation of necessary oxygen and nutrients to the tissue in the center of the stroke. The surrounding tissue might have more perfusion, thus still being reduced. As the brain have no energy reserves or ways to store energy, a constant supply of oxygen and nutrients are needed [Ovbiagele & Nguyen-Huynh (2011)]. Stroke can be divided into two categories, ischemic and hemorrhagic, depending on the cause of the stroke [Mir et al. (2014), Ovbiagele & Nguyen-Huynh (2011)].

2.1.2.1 Ischemic

Ischemic stroke is caused by insufficient blood flow to the tissue of the brain. This can be caused by thrombosis, when a thrombus develops and blocks the artery to a local region of the brain, often caused by plague buildup in the artery, an embolism, which is a part of a thrombus that breaks off elsewhere in the body and travels to the brain and block the blood flow. Lastly systemic hypoperfusion is the result of insufficient blood supply, which can be due to low circulatory blood flow. Ischemic stroke causes a deprivation of oxygen and nutrients to flow to the tissue of the brain and therefore fails to meet its energy demands. If left untreated this results in damage to neurons or necrosis within minutes of oxygen deprivation. It is estimated that 85% of stokes are caused as an ischemic stroke [Mir et al. (2014)]. Figure figure 2.3 (A) and (B) illustrates an example of ischemic stroke in the middle cerebral artery, right hemisphere, which blocks off blood flow and causes oxygen starvation in the tissue beyond the thrombus. Warning signs of an ischemic stroke often comes in the form of transient ischemic attack (TIA), which symptoms disappear after a couple of minutes or hours and lasts maximum 24 hours [Mayfield (2019)].

2.1.2.2 Hemorrhagic

Hemorrhagic stroke is caused by bursting or rupturing of a blood vessel supplying the brain with blood, which can be categorized either intracerebral or subarachnoid. This form of stroke is often accompanied with a sudden headache. Hemorrgagic stroke is the deadliest form of stroke because it often leads to an interruption of blood flow, similar to ischmic stroke, while also causing tissue compression from the blood build up. This form of stroke accounts for about 15% of all strokes [Mir et al. (2014)]. Figure figure 2.3 (C) and (D) illustrates an example of hemorrhagic stroke, (C) illustrates a ruptured aneurysm on the middle cerebral artery, left hemisphere, which is a weakened part of the artery wall and (D) illustrates bursting of the small arteries, caused by hypertension.

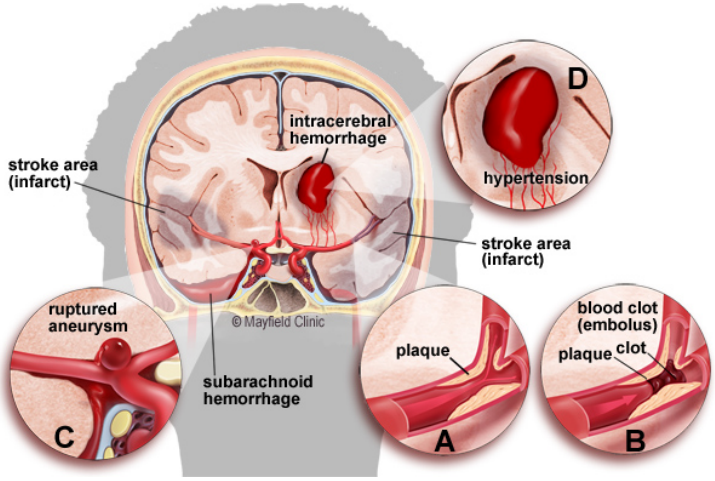

Figure 2.3: Illustration of ischemic (A) and (B), and hemorrhagic (C) and (D), stroke [Mayfield (2019)].

2.1.3 Neurological mechanisms of stroke

During the onset of stroke the brain undergoes a series of events, both destructive and protective mechanisms are involved.

Destructive mechanisms
When a stroke emerges, a number of neurological mechanisms are started by the body. The ischemic cascade is one of these, which creates local depletion of oxygen and glucose at the core of the stroke. This causes the production of adenine triphosphate (ATP) to fail because oxidative phosphorylation cannot take place without oxygen. This affects the energy dependent processes, which results in injury or necrosis of cells, because the ionic gradients across membranes cannot be maintained, as the sodium (NA^+) potassium (K^+) pump cannot function without ATP. The release of excitatory neurotransmitter such as glutamate and aspartate are triggered, which results in activation of receptors like N-methyl-d-aspartate (NMDA) and alpha-3-hydroxy-5-methyl-4-isocanole propionate (AMPA), which allows influx of sodium (NA^+) and calcium (CL^-) and water (H2O) into the already ATP depleted cells. This results in exotoxicity which results in necrosis of neuronal cells and failure of mitochondria cells. Stroke mediators of inflammation are activated by recruited leukocytes. These are in the form of oxygen free radicals, nitric oxide, cytokines and apoptosis, preprogrammed cell death. This inflammation can cause secondary damage and expansion of the stroke area, hours and days after onset [Mir et al. (2014), Endres et al. (2008)].

Protective mechanisms
Shortly after the onset of the stroke protective mechanisms are promoted in order to protect the brain from the ischemic cascade and inflammation in order to reduce damage. This is achieved by defending against necrosis and apoptosis and promoting growth of new neurons in the brain. Among these mechanisms are Bcl-2 gene family molecules and

neurotrophic factors like Neurotrophin-3. Bcl-2 gene family molecules takes part in regulating apoptosis and can inhibit the molecules that take part in the apoptosic process and by reducing mitrocondria destruction. Neurotrophin-3 is a nerve growth factor protein which helps in survival of neurons and stimulates growth of new neurons and synapses [Mir et al. (2014)].

To illustrate the destructive and protective mechanisms that follows stroke, figure figure 2.4 is provided, showing the time line of the stages for these mechanisms.

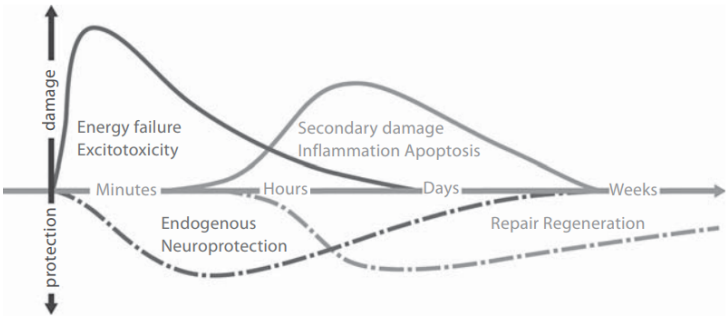

Figure 2.4: Destructive and protective timeline following stroke. On the y-axis are the condition and on the x-axis the time is displayed. [Endres et al. (2008)]

The protective mechanisms are of great importance in the regeneration and repairing of neurons and is a great example of the plastic properties of the brain, which is of great importance during rehabilitation stages [Mir et al. (2014), Endres et al. (2008)].

2.1.3.1 Rehabilitation post stroke

After the acute treated which takes place the first hours of treatment, early mobilization of the patients is initiated in the first hours and days post stroke. During these days motor, cognitive and sensory impairments are diagnosed, in order to structure a plan specific rehabilitation intervention of the patient. The following days, weeks and months the patient should follow the the rehabilitation program and adapt to the environment. Following the next month and years physical condition is maintained with regular checkups [Langhorne et al. (2011)]. Post stroke recovery can be classified as neurological recovery, which is affected by lesion site and pathogenesis of the stroke and functional, which is affected by rehabilitation consistency, environment and motivation [Lee et al. (2015)]. The neuroprotective mechanisms plays an important role in the early stages of rehabilitation as these are the most crucial for the patient in order to regain lost function and to avoid adopting bad compensatory patterns. Early rehabilitation is of great importance for patients undergoing stroke, in order to recover from their impairments as much as possible. The first one to three month post stroke is the time where the utmost changes happens in regards to factors involving neuroplasticity and remodeling of the brain [Zeiler & Krakauer (2013), Alia et al. (2017), Lee et al. (2015)]. Early mobilization and training

is put high emphasis on, when it comes to rehabilitation post stroke, because of the increased sensitivity to stimuli caused by an increase in neuroplasticity in the early stages post stroke. The study by Lee et al. (2015) showed that recovery occurred with most progression in the first three month of rehabilitation and thereafter declined until their six month follow up period. Despite increased recovery capabilities early post stroke, increased recovery outcomes has been shown with longer rehabilitation periods. This was demonstrated by the study by Cauraugh et al. (2011), which showed an increase in recovery in patients with a long term training protocol (16 month) versus patients with a short term training protocol (two month). Although the increase in recovery early post stroke, overtraining close to the acute stage of stroke may lead to expansion of the cortical lesion. This was observed from 24 hour training post stroke in rats [Summary (2000)]. The cause of tissue loss from early training can be caused by the release of glutamate, which is a necessary neurotransmitter, but oxygen deprived neurons may be vulnerable to excitation because of imbalances between excitatory and inhibitory synaptic function and the presence of ecotoxicity in the early stages of stroke. Although a bigger tissue loss early training was observed, better recovery outcomes has been linked to the early training [Summary (2000), Zeiler & Krakauer (2013)].

2.2 Neuroplasticity

Reorganization and adaptation of neural networks and pathways happens throughout the entire life. A general term for this is also know as neuroplasticity. Many machanisms are involved in neuroplasticity and it consists of a combination of ongoing processes in the body. [Augustine et al. (2004)]

During recovery the neurons of the brain are prone to reorganization through a couple of different mechanisms. When the CNS is damaged by either neurons undergoing necrosis or apoptiois, causing neural connection interruption, the potential of restoring the function of these neurons are possible trough the processes of unmasking or sprouting. Unmasking is the process in which synapses that are not efficient, which could be due to lesion, have the possibility to connect to neurons adjacent to themselves. Sprouting is the result of axons creating new connections from the damaged axon, at the site where it was damaged. [Mir et al. (2014), Thompson (2000), Taub et al. (2002)] The process of unmasking and sprouting is illustrated in a simplified way in figure 2.5, where a lesion has been induced.

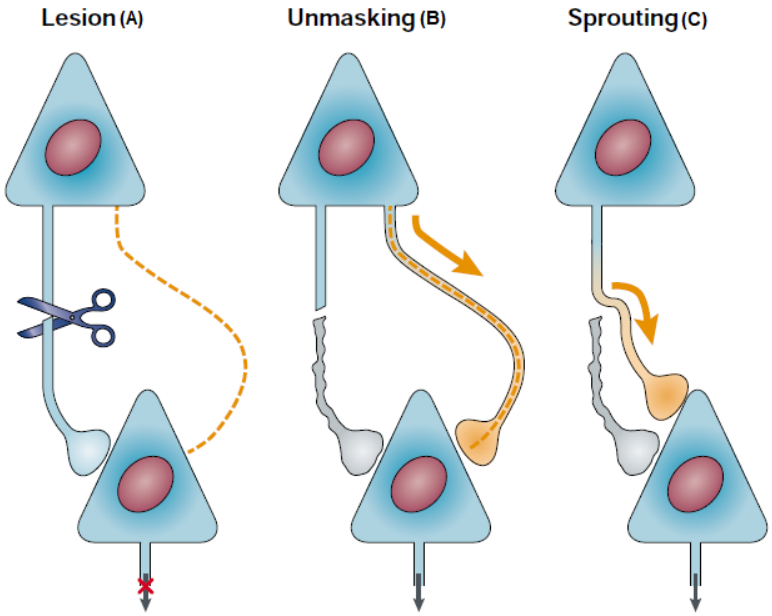

Figure 2.5: Illustrating lesion to a neuron (A), restoring of neuron function through unmasking (B) and sprouting (C) [Taub et al. (2002)]

Jordan Grafman, an American neuroscientist describes four forms of neuroplasticity. Homologous area adaptation, compensatory masquerade, cross-modal reassignment and map extension [Thompson (2000)].

- Homologous area adaptation, the process of the brains ability to take over functions by the interplay of left and right hemisphere, meaning that the right hemisphere

can take over functions from the left, and visa versa.

- Compensatory masquerade, the ability of the brain to compensate and use new strategies for problem solving, if regions of the brain dedicated to a specific function is damaged.
- Crossmodal reassignment, when the brain assigns new functions to an area of the brain, if the intended function cannot be acquired.
- Map expansion, when areas of the brain are assigned to a specific task if it is stimulated simultaneously, which makes the area to grow, resulting in enhanced task ability.

Synaptic plasticity, the ability of synaptic connections to be functionally dynamic, plays a great role in neuroplasticity and especially in cortical reorganization [Summary (2000)].

2.2.1 Synaptic plasticity

Synaptic plasticity is the ability for the synapses to strengthen or weaken the connection between neurons, dependent on the activity of the synapses. Plasticity enables the connection between neurons to be strengthened and thus enhance function.

An important form of neural plasticity when considering rehabilitation is long term plasticity, which can persists for weeks, month or even years are the mechanisms of long-term plasticity . Long term plasticity cause a long lasting change between the synapses. A long lasting strengthening of the synapses is known as long-term potentiation (LTP) while a long lasting decrease in synaptic strength i known as long-term depression (LTD). These processes happens based on different cellular and molecular mechanisms and history of activity, which is involved in procuring LTP or LTD at the synapses. It is believed that long-term plasticity is part of learning and memory linked with hippocampus [Augustine et al. (2004)].

Long-term potentation
NMDA receptors plays an important role in LTP. The opening of these channels are of great importance and can only happen at synaptic inputs that are active and release the neurotransmitter glutamate. During high frequency stimulations a prolonged depolarization in the synapse takes place. This results in mg^{2+} being expelled from the NDMA channel, allowing Ca^{2+} to enter the postsynaptic neuron. This results in increased Ca^{2+} concentration in the post synaptic neuron, which induces LTP as a second messenger signal, which in turn increases excitatory postsynaptic potentials [Augustine et al. (2004)].Figure 2.6 illustrates this process.

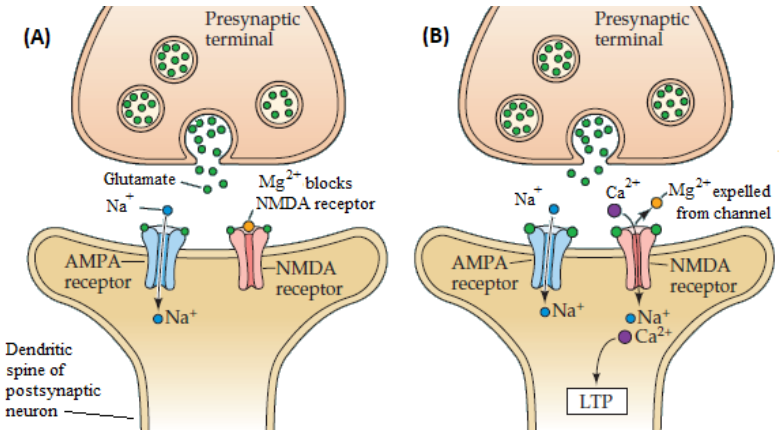

Figure 2.6: Illustaration of long-term potentiation at neuromuscular synapse. (A) mg^{2+} blocks the NMDA receptor channel. (B) mg^{2+} is expelled from the NMDA receptor channel allowing Ca^{2+} to enter the postsynaptic neuron [Augustine et al. (2004)]

Long-term depression

In order to make strengthening of synapses useful, weakening of others must take place to enhance the efficacy. LTD is this process and it takes place at low frequencies during long periods. LTD, in contrast to LTP, have the ability to reduce excitatory postsynaptic potentials. LTD is released in a similar way to LTP, by activation of NMDA-type glutamate receptors, which results in an inflow of Ca^{2+} to the post-synaptic synapse. What determines if LTD or LTP is released are the amount of Ca^{2+} in the post-synaptic synapse. Small amounts trigger LTD and large amounts triggers LTP. LTD is associated with a loss of synaptic AMPA receptors, which reduces the amount of Ca^{2+} that can enter the postsynaptic neuron [Augustine et al. (2004)]. Figure 2.7 illustrates this process.

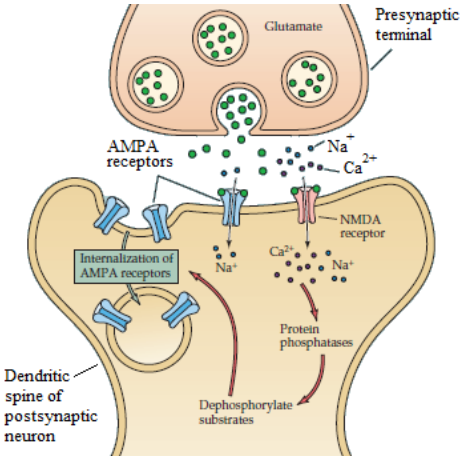

Figure 2.7: Illustaration of long-term depression at neuromuscular synapse. Low frequency of Ca^{2+} into the postsynaptic neuron activates protein phosphatases, triggering AMPA receotors. This reduces glutamate sensitivity [Augustine et al. (2004)]

2.2.2 Neurotrophic factors

Neurotrophic and nerve growth factors are of great importance during recovery of stroke. These molecules has been linked with increased memory and motor function. As briefly mentioned in section 2.1.3 Neuotrophin-3 is one of these, other nerve growth factors that has been found important during especially early recovery is brain-derived growth factor (BDNF), insulin growth factor, glia cell line-derived neurotrophic factor and transforming growth factor $\beta 1$. [Summary (2000)] A study by Peterson et al. (2012) points out that physical activity has a positive impact on neurogenesis, because it promote growth of new nerve cells from neural stem cells and release of neurotrophic factors, which both promotes neuroplasticiy. One of the nerve growth factors of great importance for the survival of neurons and motor learning and memory is BDNF, which has been shown to ease the process of LTP, one of the processes that strengthen connections between neural synapses, a part of synaptic plasticity. [Mang et al. (2013)] The study by Mang et al. (2013) found aerob excersice to increase BDNF in patients rehabilitating from a stroke and thus and enriched environment is contributing to an increase in recovery post stroke [Mang et al. (2013), Summary (2000)]. As a side note, the study by [Peterson et al. (2012)] found that stress and depression decreases recovery and thus decreases neurogenesis.

2.2.3 Adaptive and maladaptive neuroplasticity

Neuroplasticity allows the body to enhance and adapt, thus being adaptive neuroplasticity. This kind of neuroplasticity is expressed when professions that enhances our skills, like learning new motor skills or recovering from disorders like stroke Haavik & Murphy (2012). In some cases, neuroplasticity can have bad outcomes, thus being maladaptice neuroplasticity. This form of neuroplasticity can lead to disorders like phantom limb pain or movement disorders like parkinson's or dystonia. [Haavik & Murphy (2012), Takeuchi & Izumi (2012)] Recovery from stroke may cause such bad habits, why some patients develop compensatory strategies to complete daily tasks, which prevent a normal motor pattern of the injured side,thus resulting in decreased recovery [Haavik (2014), Takeuchi & Izumi (2012)].

2.3 Chiropractic

Chiropractic is a health care profession with special focus on the relationship between the CNS and the spine, why the central anatomic structures initially are outlined before the description of chiropractic is presented. This includes information about the vertebral column, the CNS and muscle spindles, as these anatomical structures have been found to be important in the effects of chiropractic SM (SM), indicated by the newest research within the field. [Haavik & Murphy (2012)]

2.3.1 The vertebral column

The vertebral column consists of 24 vertebrae, sacrum and coccyx, and is part of the axial skeleton which supports the thorax and head. The vertebral column serves the important role of housing and protecting the spinal cord [et. al. Martini (2012)]. The vertebral column is divided into the cervical, thoracic, lumbar and sacral parts, making up the spinal curve, which benefits in efficient support of the body, as external weight often is placed anterior in relation to the vertebral column. Nerve roots extend from each vertebrae, extending from the spinal cord, branching out into the peripheral nervous system (PNS), with the purpose of innervating different tissues of the body. [et. al. Martini (2012)] The prior mentioned structures are shown in figure 2.8.

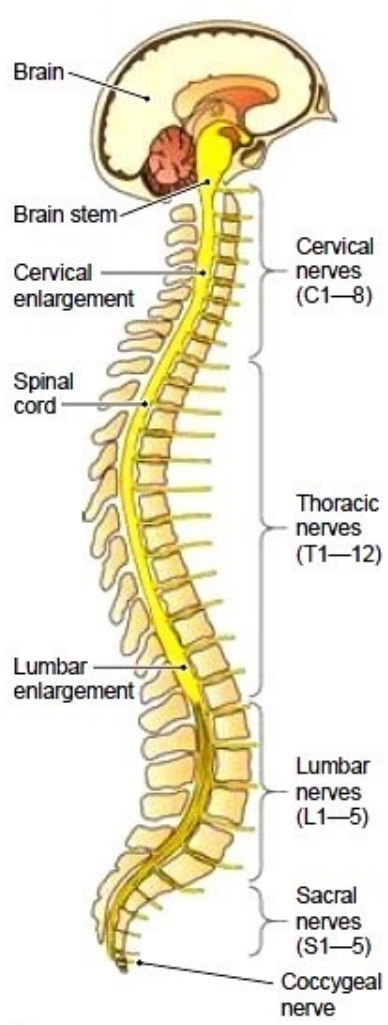

Figure 2.8: Illustaration of the vertebral column and CNS, lateral view. Modified from [HEBA SOFFAR (2018)].

Each vertebra are connected by three joints. One of these is the intervertebral disc, which separate and act as shock absorber between vertebral bodies. The other joints are the facet joints, with the function of limiting movement of vertebrae segments. [Haavik (2014), et. al. Martini (2012)]. A popping sound is often a characteristic during SM. This is caused by gas release of the facet joints [Haavik (2014)]. The muscles that stabilize and support the vertebral column, hence each vertebrae, are the semispnalis group, multifidus and interspinales, intertransversal and rotators [et. al. Martini (2012)]. These muscles makes up the paraspinal muscles, not only important in spinal support, but also in perceiving proprioceptive information from the muscle spindles. [Haavik (2014)]. Figure 2.9 illustrates a section of the vertebral column (A) and the paraspinal muscles that attaches to the vertebrae (B).

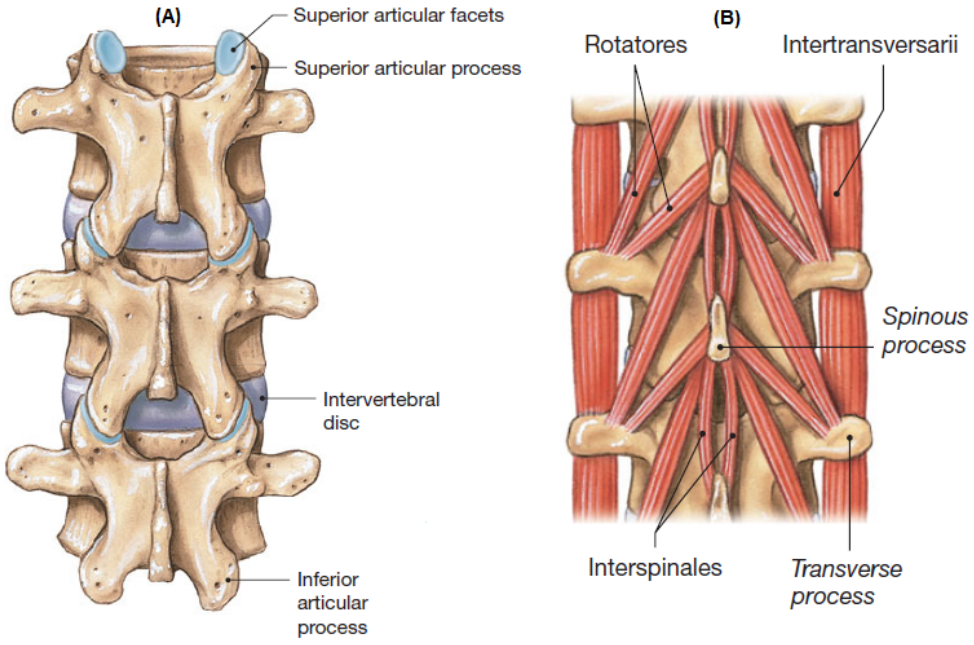

Figure 2.9: Illustration of intervertebral disc and facet joints from a part of the vertebra, posterior view (A). Illustration of the paraspinal muscles of the vertebral column, posterior view (B). Modified from [et. al. Martini (2012)]

2.3.2 Muscle spindles

Muscle spindles are specialized stretch reflexes, sensing changes in muscle length. They consist of always active intrafusel muscle fibers, sending sensory information via afferent nerve fibers to the CNS. This allows the body to monitor the activity of the muscles in the body, by sensing how much the muscle spindles are stretched, which plays an important role in proprioception. The mechanism of the muscle spindle works by increasing the frequency of action potentials, when the stretched and decreases when decompressed. The information goes the spinal cord via the afferent nerve fibers of the muscle spindle, stimulating Alpha motor efferent neurons, making the extrafusal muscle tissue contract, as a protective mechanism. The CNS adapts the sensitivity of the muscle spindles via the gamma motor efferent neurons of the muscle spindle. [et. al. Martini (2012)].

Muscle spindles and the stretch reflex plays a great role in proprioception as mentioned, examples of this are posture and cooperation between agonist and antagonistic muscle groups, ensuring an upright posture and even balanced body during movement. This is achieved by sensitive stretch reflexes and their ability to keeps a firm muscle tonus. [et. al. Martini (2012)]. The mechanism in which this is achieved is also denoted feedback control. Proprioception is the ability to get information about the state of position and hold this up against a desired state. Disturbances from the external environment will influence muscle tonus in order to compensate for the changing environment and to maintain the

desired state. Another mechanism known as feed-forward control is utilizes in the case of rapid movement and information about external environmental factors are registered beforehand in order to prepare the feedback control mechanism, which could be achieved through vision or past experience, why brain regions like the hippocampus and prefrontal cortex are activated [Preston & Eichenbaum (2013), Ghez & Krakauer (2000), Kolb et al. (2012)].

2.4 Definition of chiropractic

Chiropractic is defined by the world health organization as "A health care profession concerned withh the diagnosis, treatment and prevention of disorders of the neuromusculoskeletal system, and the effects of these disorders on general health" [Salehi A et al. (2015)]. The first theories on chiropractic hypothesized that nerve roots where being compressed from misaligned vertebrae. The hypothesis has been changed several times and the latest research are showing the the muscle spindles of the paraspinal muscles plays a role in the effects of chiropractic treatment. It is thus being hypothesized that the effects of chiropractic SM is caused by stimulation of the muscle spindles of the paraspinal muscles, resulting in improvement in health and wellbeing from altered proprioceptive input. [Haavik (2014), Robert F. Schmidt & Gerald F. Gebhart (2013), Horowitz (2007)]. The segments of the vertebral column that are being adjusted are characterized as vertebral subluxations, which are causing the joints of the vertebrae to be unable to move in their full range of motion, thus the muscles paraspinal muscles cannot be stretched properly. This is believed to causing interference in the afferent nerve signaling and thus creating imbalance in the communication between the spine and the CNS. [Haavik (2014)]. During a chiropractic session vertebral subluxations are identified through palpation of the vertebrae and inspection of the patient, in order for the chiropractor to know how to adjustment the patient through SM. From high velocity, low amplitude trusts, which is the essence of SM, triggers a reflex response in the muscle spindles, which is thought to reset the muscle spindle and restores muscle tonus of the external muscle tissue [et. al. Martini (2012), Haavik et al. (2018), Pickar (2002)]. Causes of vertebral subluxations can be explained by the paraspinal muscles which stabilize the vertebral column. Tight or stiff muscles are believed to create imbalances in the joints of the vertebrate and improper proprioception from the muscle spindle related to the muscle. The improper proprioception is caused by improper movement of the vertebral joints. Physical injury, bad posture or stress, can all contribute to segments of the vertebral column to become subluxated [Haavik (2014)]. Tight paraspinal muscles might pull on bones of the vertebral column in an uneven way, which induces a stiff or misalignment joint, resulting in abnormal movement of the joint, which affects the somatosensory signaling from the muscle spindles [Haavik (2014)]. Information from muscle stretch sensed by the muscle spindles is highly important in sensorimotor integration for precise and coordinated movement, while also serving as a protective mechanism for spinal stability [et. al. Martini (2012)]. If the muscle cannot be stretched properly, the vertebrae related to that muscle is likely subluxated, as this segment is not able to move in its full range of motion, which in turn can lead to maladaptive plasticity, explained in section 2.1.3.1. [Haavik & Murphy (2012)] Through

SM muscle spindles are stimulated and altered in order to gain normal functionality, illustrated in figure 2.10. [Pickar & Kang (2006), Fritz et al. (2011)]

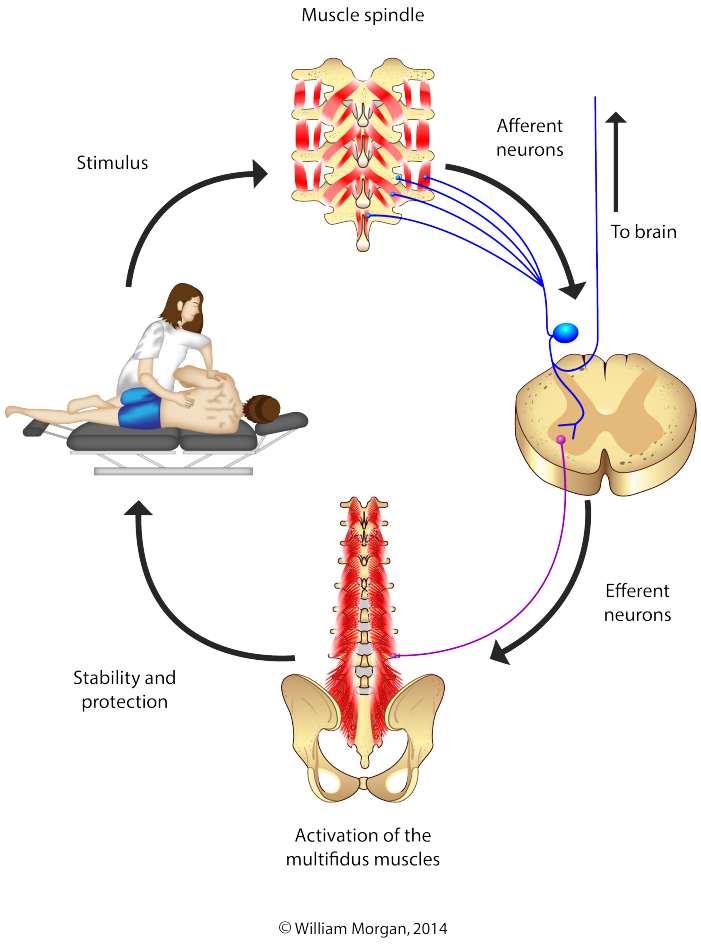

Figure 2.10: Illustration of how the muscle spindles of the paraspinal muscles are stimulated during chiropractic SM, from high velocity, low amplitude thrust [Morgan (2014)]

.

The most practiced form of chiropractic is the so called diversified technique, where the technique involved applying high-velocity, low amplitude thrusts to the spine, delivered in under 200 ms, in order to improve and restore movement of subluxated joints [Blum (2002)]. Other practiced forms of chiropractic utilizes different equipment to assists in the adjustments, like the Gonstead or Thompson technique, which uses a special table or the activator method, where a spring loaded hand held tool are used. [Blum (2002)] Techniques are often practiced in combination in order to support each other. [Haavik (2014), Sung et al. (2005), Pickar & Kang (2006)].

Research show that SM has an effect on the CNS, by altering somatosensory processing and early sensorimotor integration from afferent input perceived from the muscle spindles. A hypothesized model that describes the effect and idea of chiropractic SM are described by Haavik & Murphy (2012). The model describes the effects of postponed vertebral subluxations and basic consequences of this, where maladaptive neuroplasticity may play a role in leading to bad function. This is illustrated in figure 2.11.

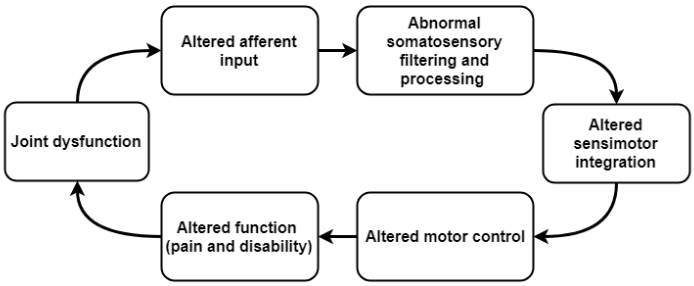

Figure 2.11: Illustration postponed joint dysfunction, which leads to altered motor function. Modified from [Haavik & Murphy (2012)]

.

By inducing the intervention of SM, normal function of muscle spindles are achieved and the patient will enhance in several ways by correcting vertebral subluxations, which further has benefits to health and wellbeing, because proprioception is precieved in a proper way from the muscle spindles. [Haavik & Murphy (2012)] This is illustrated in figure 2.12.

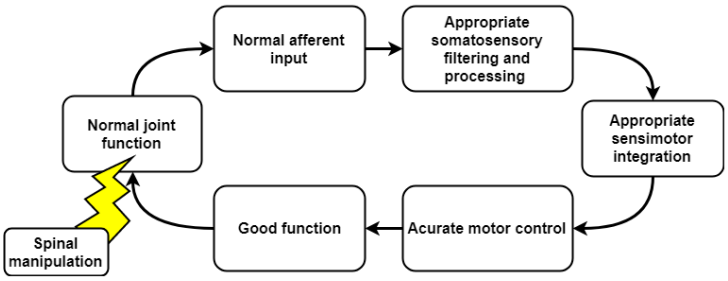

Figure 2.12: Illustration of joint dysfuntion, which is taken care of through SM, thus promoting normal function of the nervous system. Modified from [Haavik & Murphy (2012)]

2.4.1 Applications for chiropractic

Chiropractic care has shown beneficial in treating conditions of pain, especially back and neck pain and also headaches. Other effects that has been observed from chiropractic care are muscle relaxation, improved muscle coordination, improvement in posture, mechanical stress on joints reduction and degeneration reduction [Horowitz (2007)]. These benefits can all be due to enhanced neural function and it has been shwon that chiropractic care can improve reaction time, reflex excitability, joint position sense error, cortical

processing, motor control, lower limb muscle strength and cortical sensorimotor integration [Lelic et al. (2016), Haavik & Murphy (2012), Niazi et al. (2015)]. Every age group can benefit from chiropractic and is well considered in regards to proactive treatment. Other application for chiropractic are being investigated, for instance the possibility of application in rehabilitation in patients with motor disabilities, like stroke or Parkinson's disease. [Haavik (2014), Lelic et al. (2016), Khlebopros (2015), Sell et al. (2012)]

2.4.2 Chiropractic and neuroplasticity

Neuroplasticity induced changes have been linked with SM by several studies [Haavik et al. (2018), Christiansen et al. (2018), Johnson (2013)]. The research suggests that CNS nerve signaling is modified following SM, explained by altered proprioceptive input to the brain [Haavik (2014)]. This is for instance found through modified sensorimotor integration and increased maximal bite force in patients suffering from subclinical neck pain [Johnson (2013), Haavik et al. (2018)]. Previous studies performed on animals show that altered sensory input affects muscle activity [Morimoto et al. (1989)]. It is suggested that this effect could be the result of altered cerebellar output to motor cortex areas, thus enhancing movement pattern quality and force production [Johnson (2013)]. These findings are confirmed a study by Lelic et al. (2016), which also shows alterations in early sensorimotor integration following SM. An interesting finding is that the same study found these alterations of early sensorimotor integration mainly in areas of the prefrontal cortex. The study by Niazi et al. (2015) demonstrate muscle strength increase in planer flexor muscles. These finding was explained by increased spinal alpha-motoneurons excitability and reflects transmission efficiency, indicated by altered H-reflex response and increased efferent motor output magnitude from the alpha-motoneuron pool, indicated by altered V-wave. Both H-reflex and V-wave has been shown to be altered from resistance training, showing increased V-wave and H-reflex amplitude. The strength gains following resistance training might not originate from increased cross sectional area of the muscle, but rather an increased neural drive to muscle fibers [Aagaard et al. (2002), Vila-Chã et al. (2012), Dalgas et al. (2013)]. A recent study by Holt et al. (2019) showed that patients suffering from chronic stroke gained increased plantar flexor muscle force production following single session SM, along with H-reflex and V-wave threshold increase. The patients participating in the study had suffered from stroke for a minimum of 12 month and showed symptoms of planter flexor muscle weakness. It is thought that these results was obtained as a result of modulation of neuroplasticity, which could be caused by cortical plastic reorganization in relation to increased cortical drive to the muscle, as the SM had an impact in preventing maladaptive neuroplasticity and improvements by correcting vertebral subluxations, improving spinal function [Haavik & Murphy (2012), Taylor et al. (2010)]. The study by Gay et al. (2014) looked at pain perception and functional connectivity following manual therapy, including SM, showed that functional connectivity increased as an immediate effect of the treatment, along with a decrease in pain perception. The authors of the previous mentioned study suggests that changes within the nervous system is altered by SM, which may play a role in pain relief effects.

2.4.3 Methods for investigating mechanisms of spinal manipulation

The ability to measure neurolasticity is important in determining neurological recovery. Neuroplasticity can be observed by utilizing different measuring techniques that record the activity of the brain from either structural or functional changes. Structural changes refer to the structure and thickness of gray matter density, while functional changes refers to neural activity between neurons. [Warraich & Kleim (2010)] Popular techniques are positron emitted tomography (PET), single-photon emission computerized tomography (SPECT), functional magnetic resonance imaging (fMRI), electroencephalography (EEG) and magnetoencephalography (MEG). Every technique have their benefits and drawbacks. Spatial and temporal resolution, invasiveness and price varies dependent on the technique. EEG has shown to have good temporal and descent spatial resolution and the cost is reasonably low compared to the other techniques while also being non-invasive. EEG measurement makes it possible to measure neuroelectrical potentials, which can be used to measure functional changes in the brain. One technique to achieve this is functional brain connectivity analysis, which measures the functional connections between brain regions. Prior studies have been using this technique in order to asses recovery in stroke patients and changes in relation to neuroplasticity. [Lystad & Pollard (2009), Westlake & Nagarajan (2011), Wu et al. (2015)] Markers of reduced efficiency in sensorimotor signals has been shown by reduced connectivity between nodes of the cortical motor system of the cortical motor cortex M1 (FC3 and FC4) and frontal premotor cortex PM (C3 and C4) of the stroke hemisphere in post stroke patients [Wu et al. (2015), Rosjat et al. (2016)]. Results from functional brain connectivity analysis in fMRI studies have also shown reduced connectivity across the stroke hemisphere of cortical motor area during movement motor deficits and reduced connectivity between stroke hemisphere M1 and non-stroke hemisphere M1 post stroke, which increases after therapy. It is thus likely that measures of cortical motor connectivity can contribute as a biomarker of post stroke sensorimotor signal function and neuroplasticity [Wu et al. (2015)].

2.5 Functional brain connectivity

Functional brain connectivity is a measure by means of statistically estimated connection and shared changes between regional neural activity of the brain [Ni & Chen (2012)]. Functional connectivity can thus be represented as a network, expressing the coupling between brain regions, using measurements from modalities like PET, fMRI, MEG and EEG. [Manuscript (2013)]. Task performance functional connectivity is one application where functional connectivity is utilized for task performance assessment. In the recent research resting state functional connectivity has become more popular in studying functional brain organization [Chen et al. (2015), Puig et al. (2018), Gay et al. (2014)]. This method benefits from it not requiring the participant to perform specific tasks and are therefore well suited for experiments where participants might have impairments, which can make task performance difficult [Ni & Chen (2012)]. Several studies have utilized resting state data in order to study functional connectivity in stroke suffers [Chen et al.

(2015), Puig et al. (2018)]. Especially the well studied resting state network, the default mode network (DMN) are of special interest when studying resting state data [Smith et al. (2018*a*), Van Den Heuvel & Pol (2011)]. The DMN are made up of connections between specific brain regions which has been shown to be especially active during rest and less active during task related work, in healthy participants. The involved regions of the brain are the precuneus, medial frontal, inferior parietal cortical and medial temporal regions of the brain [Van Den Heuvel & Pol (2011)].

There are several ways of calculating functional connectivity, Coherence and Phase Locking Value (PLV) are examples of methods in the frequency domain and correlation and Mutual Information (MI) are examples of methods in the time domain of possible ways to obtain functional connectivity networks from modalities like EEG [Manuscript (2013)]. Both correlation and covariance only accounts for linear dependencies between variables, but as EEG signals often exhibit a complex form of nonlinear properties MI and PLV are well suited for analysis of such signals as these measures also take non-linear interactions into account [Wang et al. (2009), Sakkalis et al. (2006)]. MI accounts for both linear and non linear dependencies, meaning that these methods can give a measure of coupling between two signals and does not make assumptions about linearity while also providing stable estimates with data sets of reasonable length. MI also allows for narrow frequency band analysis, which can be used to determine different spectral bands. [Ramanand et al. (2011), Sakkalis et al. (2006)] Studies utilizing MI analysis on EEG signals have investigated patients suffering from conditions like sleep deprivation, Alzheimer's disease and depression, whom also showed lowered information of functional connectivity across specific brain regions [Ramanand et al. (2011), Ming et al. (2018)]. EEG signals recorded from scalp makes for a problematic dilemma, as these signals often are affected by volume conduction and field spread, where signals originating from the same source are being picked up from the adjacent electrodes Lai et al. (2018). Several methods exist to solve these problems, including EEG source reconstruction and using functional connectivity metrics that are robust to these effects. A variation of the PLV, known as Phase Lag Index (PLI) are among these Colclough et al. (2016). These aspects will be elaborated in the method section 3.2.1.

2.6 Problem statement

Stroke is a global problem with devastating consequences for the patients, as it affects life quality negatively. Stroke survivors often have to deal with disabilities of varying degree post stoke. Rehabilitation is therefore of great importance in order to the maximize successful recovery. During stroke, highly degenerative processes and cascades are initiated in the brain which causes damage to the stroke site which lack oxygen and nutrients, but protective mechanisms are also initiated by the brain to minimize damage and promote recovery post stroke. Neuroplasticy is one of these processes and it plays a big role in recovery and is essential for optimal recovery and regaining lost functions in utilizing new task execution strategies for the brain. A growing body of research is being conducted to empirically show the effects of chiropractic SM and what mechanisms that drives these

effects. Several studies have already shown that chiropractic SM alters neural pathways at the level of the CNS, thus inducing neuroplasticity. This is indicated by altered areas of the prefrontal cortex, reduced pain sensitivity and cortical drive following SM [Johnson (2013), Lelic et al. (2016)]. Increased force production has also been linked with single session SM by several studies, also in stroke patients [Niazi et al. (2015), Haavik et al. (2017), Holt et al. (2019)]. Despite these findings, the effects of SM are not fully investigated, especially not the mechanisms related to neuroplasticity in patients suffering from conditions like stroke or other neurological diseases. The effects of SM therefore still needs further research in order to establish evidence on how it affects the body, especially the CNS, in order to find purpose of chiropractic care and implications in rehabilitation settings relating to stroke. Non-invasive methods such as EEG functional brain connectivity analysis can be a useful tool in analyzing how brain regions communicate between each other, both during task performance and at rest, through the analysis of MI and PLI connectivity metrics and thus give an estimate of brain function and recovery post stroke.

2.6.0.1 Aim

The aim of this study is therefore to explore the effects of chiropractic SM by utilizing the method of MI and PLI to estimate resting state EEG functional brain connectivity, in chronic stroke patients.

3 | Material and methods

3.1 Subjects

24 chronic stroke patients were recruited to participate in the experiment, all male, mean age, 54.9 ±11.4. The patients had suffered from stroke for a period between 2 and 60 month, mean 18.2 ±14.4 months. Location of the stroke varied between patients. The affected hemispheric region of the brain was distributed as 13 right hemispheric and 11 left hemispheric affected, all of ischemic stroke type.

3.1.1 Spinal manipulation session

Vertebral subluxations where assessed in the subjects before and after performing SM by inspecting the whole spine along with the sacroiliac joints, performed by a New Zealand registered chiropractor. Indicators of vertebral subluxaions was found by manual palpation and characterized as restricted intersegmental range of motion, intervertebral muscles asymmetric tension, restricted range of motion of intersegmental vertebrae, joints tenderness to palpation and other abnormal joint play. High velocity, low amplitude thrusts or instrument assisted adjustments were performed during the SM adjustments.

3.1.2 Control session

During the control session the subjects was examined according to the procedure of the SM session and moved into the adjustment position but without performing any adjusting thrusts. This procedure was performed to account for changes which could happen due to muscular, cutaneous or vestibular effects in the SM session. This procedure was done between Pre and Post recordings by the same chiropractor, similar to the study done by [Holt et al. (2019)].

3.2 Experimental protocol and equipment

The conducted experiment were carried out as a randomized crossover study design where each participant participated in control and SM session. In order to reduce bias like carry over effect, all subjects were randomly allocated into one of the intervention in order to determine their first session, before the experiment was initiated. A washout period of at least one week was given to the subject between experimental sessions. An overview of the of cross over study design is illustrated in figure 3.1.

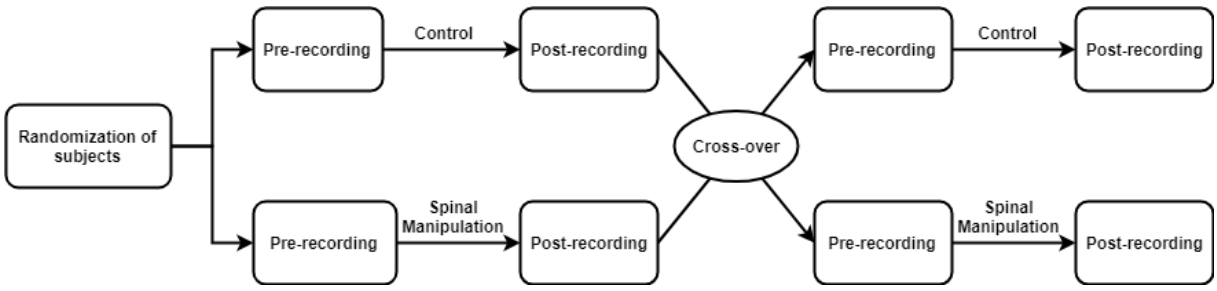

Figure 3.1: Illustration of the cross over study design and recording allocation.

Resting state EEG signals were recorded for all subjects during two consecutive sessions pre and post intervention of either control or SM. For recording of the EEG signals, a Refa 72 channel TMSi device (The Netherlands) was used, connected to a 64 electrode EEG cap which was placed on the scalp of the subject according to the extended 10-20 system [Siuly et al. (2016)]. Furthermore the setup was connected to ground through electrode at location F_Z, see figure 3.2. Impedance were below 10 ohm. A computer were used for storing and acquiring the data. The recording setup were powered by a battery source in order to minimize power line noise. During the EEG acquisition the subjects where positioned sitting comfortably in a chair asked to sit still with eyes open and relaxed keeping the gaze on a cross located on the wall 1.5 meters opposite to the participant. Two to three minutes of of resting state EEG was acquired during each session, were subjects were asked to keep movement and eye blink minimal. Sampling frequency of 2048 Hz. After a washout period of at least seven days the subject repeated the experiment with the second experimental session in the cross-over design. Data recordings was carried out at Railway General Hospital in Rawalpindi, Pakistan, between 2016 and 2019, by researchers from the New Zealand College of Chiropractic.

3.2.1 EEG acquisition

EEG is a non invasive measurement method, which measures electrical postsynaptic potential activity, generated by pyramidal neuron cells making electrical dipoles between soma and apical dendrites in the brain. These potentials can be measured by electrodes placed on the scalp. EEG is most often recorded as a multichannel signal with electrode numbers ranging from 1 to 256 parallel recordings, where one electrode is referred to as one channel [Im (2018), Siuly et al. (2016)].

Electrode placement are of great importance as each electrode is responsible to record signals from different brain regions. Standards have been made in order to achieve standardized measurements of EEG signals, the international 10-20 electrode placement system is one of those, which is shown in figure 3.2 and the one used in during the recordings of the EEG signals in this project. Even numbers indicates the right hemisphere and odd numbers indicates the left hemisphere location [Siuly et al. (2016)].

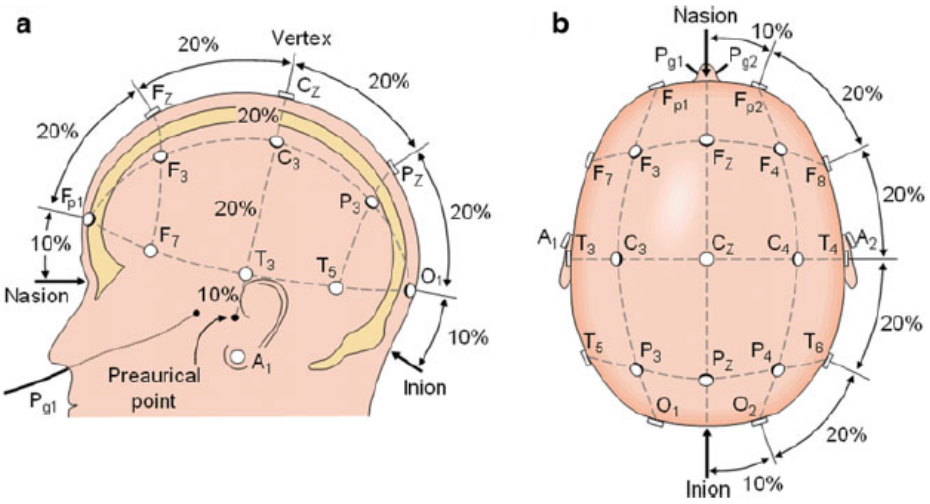

Figure 3.2: Illustration of the 10-20 electrode placement system setup on the scalp [Siuly et al. (2016)].

Recording can take place as either bipolar or unipolar montage. During bipolar montage, electrode pairs are recorded as the potential difference between electrodes adjacent to each other, while during unipolar montage, electrode channels are represented for each electrode with a common reference, desirably placed at a midline position in order to avoid amplification in one hemisphere over the other [Im (2018)]

3.2.2 Characteristics of the EEG signal

, The amplitude of EEG signals ranges from 1 to 100 uV and the frequencies of the EEG signal is contains meaningful information about changes and status of the brain. Oscillatory waves of the brain are often divided into the following frequency bands, typically defined in the ranges, Delta (1.3-3.5 Hz), Theta (4 - 7.5 Hz), Alpha (7.5 - 12.5 Hz), Beta (12.5 - 30 Hz) and Gamma (30 - 40 Hz) Newson & Thiagarajan (2019). Delta waves is an expression of sleep, serious brain disorders and waking state [Im (2018), Siuly et al. (2016)]. Theta waves expresses emotional stress, frustration and disappointment. Alpha waves indicates activity in posterior regions and often happens in the occipital lobe during relaxed state, intense mental activity, stress and tension. The alpha waves are also linked with sensorimotor areas. Beta oscillations often happens in the frontal lobe and are associated with arousal and are actively engaged in mental activities, attention and outside focus along with problem solving tasks. Lastly are the gamma osculations, which expresses cognitive and motor function, these waves can have frequencies up to 100 Hz [Siuly et al. (2016), Im (2018)].

3.3 Data analysis

Offline data analysis was conducted in MATLAB R2018a. Toolboxes used during the analysis were, EEGLAB version 14.1.2 for preprocessing, Brainstorm version May 2019 for source reconstruction and EEGNET version 1 was used for network visualization in the cortex.

Initially a pipeline of the methodological approach for the data analysis is outlined in order to give an overall overview, this is illustrated in figure 3.3.

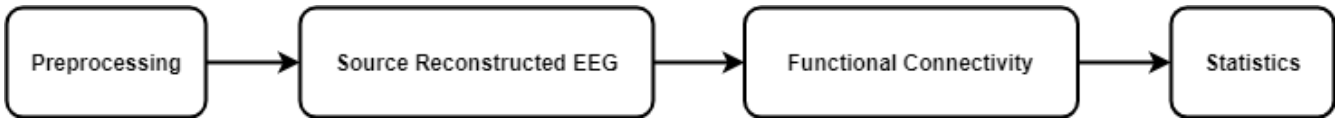

Figure 3.3: Pipeline illustrating the steps performed during the data analysis.

The following chapters will contain further explanations of the approaches for each of step performed during the data analysis from the pipeline in figure 3.3.

3.4 Preprocessing

The EEG signals both contain the desired signals originating from the postsynaptic potentials generated by the neurons, but the electrodes also pick up signals in the form of artifacts from non-cerebral origin. Artifacts are always very likely to contaminate the EEG signals and can disturb further analysis and interpretation of results, therefore preprocessing of the signals are needed in order to enhance signal to noise ratio. Well known artifacts in EEG arises as line noise, eye movement, blinks and generally excitation of the facial muscles and muscles of the of the eyeball. Bad electrode contact are also a cause of artifact as this leads to high impedance between skin and electrode [Im (2018)]. In order to remove these artifacts and prepare the signals for further analysis, a pipeline for the pre-processing are outlined and illustrated in figure 3.4. Preprocessing of the data was done using EEGLAB, where data was loaded into and channel locations were defined before the initialization of the preprocessing steps.

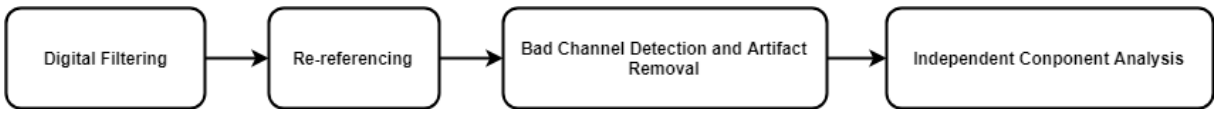

Figure 3.4: Illustration of the steps performed during the pre-processing of the EEG signals.

3.4.1 Digital filtering

Digital filtering of the EEG signals were applied in order to remove linear trend and unwanted line noise originating from signals picked up from connectors and cables, main

supply connected devices and devices in the same circuit as the amplifier, which allows propagation of noise to the recording setup. This noise often show itself at frequencies at either 50 or 60 Hz along with its harmonics [Cutmore & James (1999)]. A spectrum analysis of the EEG signals revealed that most of the signals were contaminated with 50 Hz noise and its harmonics, in varying degree. A digital bandpass filter of zero phase finite impulse response (FIR) was applied to the signals using a windowed hamming. The filter were defined with the bandwidth 1 - 45 Hz of order specified automatically in EEGLAB by a heuristic process, which determines the order based on the high edge frequency and sampling rate. When these parameters were defined the default filter order in EEGLAB was 6760, with transition band width of 1 Hz. The bandwidth of 1 - 45 Hz was chosen because the frequency range of interest lies between 8 - 40 Hz, thus removing line noise along with linear trends and high frequency components, which will not be included in the further analysis. The narrow frequency range also made preprocessing more convenient in regards to artifact removal, which is one of the later steps in the preprocessing pipeline.

3.4.2 Re-referencing

During the recordings of the signals in the experiment, monopolar recordings was obtained using the mastoids for reference electrodes. Another option is to use a common average reference for all electrodes, which is using the averaged sum of the electrode output, as positive and negative currents will sum to zero, when summed across electrodes, according to ohm's law. Even distribution of electrodes over the scalp are assumed. Average reference is often used as potential difference varies on the scalp [Siuly et al. (2016), Im (2018)]. During the preprocessing, re-referencing was done to achieve common average reference, excluding the two mastoid references, leaving 62 electrodes for further analysis.

3.4.3 Bad channel detection and artifact removal

Artifacts og disturbances in the EEG signals originate from both internal and external sources. Internal sources are from physiological systems, including electrical interference emanating from the heart, eyes and muscles, while external sources include all other signals from environments which can contaminate the signal. These include wireless device, electronic devices, wires, etc [Im (2018), Siuly et al. (2016)]. Before artifact removal, bad channels where marked using EEGLAB plug-in *clean_rawdata*, which marks the data by searching for flat line, noisy signals with excessively large amplitudes or poorly correlated to neighboring channels. The channels marked as bad were manually inspected, validated and excluded if the channels where considered bad [Chang et al. (2018)].

Artifact subspace reconstruction (ASR) is a part of the $clean_rawdata$ plug-in in EEGLAB and were used to mark artifacts in the data. The way that ASR works is by initially selecting parts of the data that are considered clean, as calibration data. This selection is based on distribution of signal variance, by calculating channel-wise root mean square. A principal analysis sliding window analysis is then performed based on z-score statistics

to find high variance signal components which exceed a user defined threshold of 200 relative to the covariance of the calibration data Manley (2013), Mullen et al. (2015), Pedroni et al. (2018).

The threshold of 200 was chosen on the bases of the study by, which mentions that a mild threshold of 100 or above is preferred. Lastly the signals determined by the ASR algorithm was removed after visual inspection, in order to validate the the marked artifacts[Chang et al. (2018)].

After rejection of bad channels and artifact removal, channel count would be unequal for individual subjects which would be cause of error if not handled [Hatz et al. (2015)]. Therefore the removed channels where reconstructed using spherical interpolation where information from neighboring channels were used for reconstruction after artifacts were removed [Bigdely-Shamlo et al. (2015)].

3.4.4 Independent component analysis

Independent component analysis (ICA) is method used in blind source separation (BSS) and is an often used method to remove artifacts in the EEG signal [Hatz et al. (2015)]. ICA are based on either second or higher order statistics and assumes mutual linear independence between estimated sources along with non-Gaussianity. In BSS a linear mixture model is used in which the observed multi-channel EEG signals are assumed to be a linear mixture of unknown sources with little knowledge about sources or a mixing matrix. Assumption about mutually independence are made in order to achieve optimal source and mixing matrix estimation. If we have an observed EEG signal $x(t)$, this can be explained as a mixture of an unknown source vector s with mixing matrix A and white noise n [Im (2018)].

$$x(t) = As + n \tag{3.1}$$

Sources can then be made as independent as possible by estimating A, to obtain the inverse matrix given by

$$W = A^{-1} \tag{3.2}$$

This inverse matrix can then be used to find the sources by the equation.

$$s = Wx \tag{3.3}$$

Before computation of ICA, the EEG signals were down sampled to a sampling rate of 512 Hz, in order to optimize computation efficiency. The IC components were semi automatically marked as bad or good components using Multiple Artifact Rejection Algorithm (MARA) to mark bad components [Pedroni et al. (2018)]. MARA is an opensource EEGLAB plugin, based on a supervised machine learning algorithm, which automatically labels the independent components for artifact rejection. The components were visually

inspected and verified before removal. MARA classifies EEG signal components and artifact components, based on a supervised learning algorithm which has been trained from expert ratings of 1290 components, six features are considered from spectral, spatial and temporal domains. IC components that are considered bad and originate from artifact components are subtracted from the data, leaving the good EEG components, which are considered making up the features of the EEG signal [Islam et al. (2016), Pedroni et al. (2018)].

3.5 Sensor level EEG

EEG sensor level connectivity analysis have its limits, as problems like volume conduction and field spread arises, because common signals are being picked up by adjacent electrodes on the scalp [Rutkove (2007)].The term volume conduction describes the effects of measuring electrical potentials at distances from where the source originates, because the electrodes that are recording the signals are not directly placed to contact the nerve at the specific location which are being measured. Far field potentials and near field potentials are considered when considering volume conduction. Far field potentials are generated a distance from the recording electrodes, while near field potentials are obtained close to the recording electrode and the source of interest [Rutkove (2007)]. Interpretation of sensor level EEG can for this reason be problematic, as the recordings are affected by the effects of volume conduction . Ideally connectivity between two physically-distinct brain regions would be if the electrodes only measured the neural activity right below the electrodes. But as the sensor signals are an expression of complex mixture of overlapping signals from a number of brain regions, this ideal scenario cannot directly be achieved [Hassan & Wendling (2018)]. Sensor level EEG measures all sources at a certain degree, depending on the source to sensor distance and orientation of equivalent dipoles associated with the sources. Figure 3.5, illustrated the problem of volume conduction, showing an ideal scenario and what is the reality.

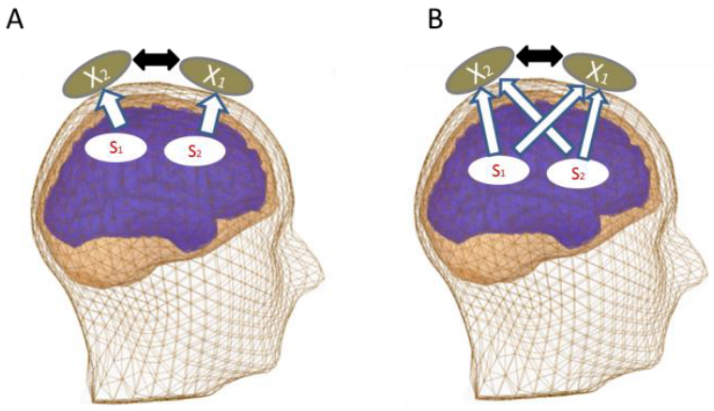

Figure 3.5: Illustration of the volume conduction problem. A) Ideal scenario, each electrode picks up signals only related from sources generated at a specific brain region. B) Volume conduction occurring due to signals from different sources are being picked up from multiple electrodes [Hassan & Wendling (2018)]

In order to solve the problem of volume conduction, one solution is to do EEG source reconstruction from the recorded sensor level EEG [Hassan & Wendling (2018), Im (2018)].

3.6 Source level EEG

EEG source reconstruction is a strategy to solve the the problem of volume conduction and also enhances the spatial resolution of the data, as the cortical activity are being reflected as sources reflecting dipoles, instead of sensors reflecting the mixture of multiple source signal. EEG source reconstruction is a process where location, direction and distribution of EEG sources are estimated by solving forward and inverse mathematical problems. This includes a procedure where modeling of the head and relationship between the EEG sources and scalp potentials are being approximated [Im (2018)]. EEG source reconstruction consists of two main problems, forward modeling and inverse modeling, which are dependent on each other for correct source reconstruction. Forward modeling involves the calculations and modeling of the human head, including scalp, skull and cortex and sensor array electromagnetic properties, while the inverse problem uses information from the forward modeling problem in order to identify most likely locations and strengths of cortical activity [Tadel et al. (2011), Im (2018)].

3.6.1 Source reconstruction

To do EEG source reconstruction four essential pieces of information are needed, the sensor EEG signals, information about the electrode placement on the head in 3D space, a head model containing information about electrical and geometric characteristics of the head and a model which provides information about the location and orientation of dipole sources that is being estimated [Hassan & Wendling (2018)]. Figure 3.6 illustrates the four pieces needed in order to achieve EEG source reconstruction.

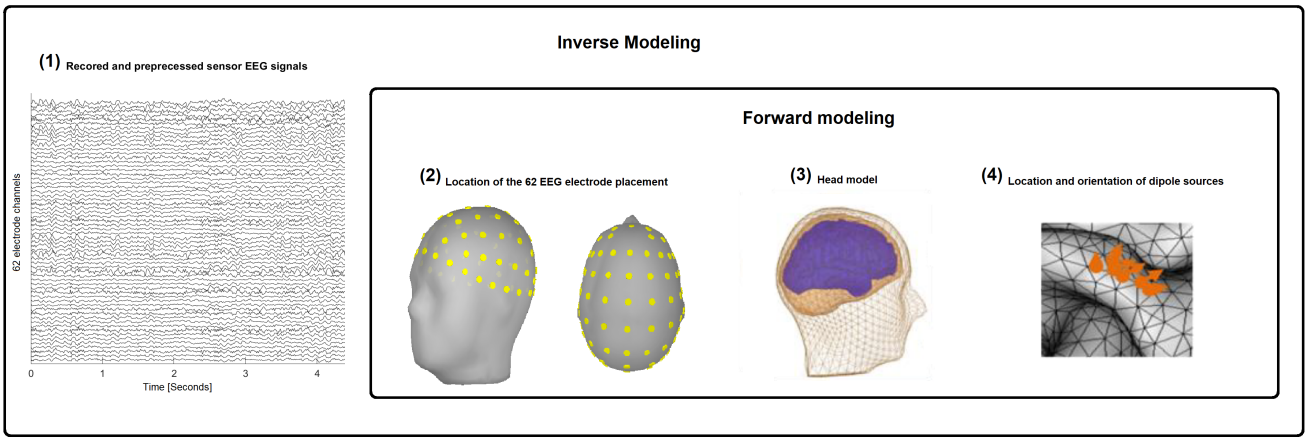

Figure 3.6: Illustration of the four essential pieces of information needed to do EEG source reconstruction. (1) illustrating the EEG sensor time series, (2) the electrode placement, (3) the head model, (4) dipoles location and orientation. Modified from [Im (2018)].

Post synaptic potentials generated in cortical pyramidal neurons of cerebral cortex are assumed to be orientated approximately normal to the cortex, which is assumed in the model and it is the mass effect of these cells are being modeled. This can done on a spatial level by making up electric current dipoles, which are distributed along and perpendicular to the cortex, which then will represent an approximation of the brain activity [Im (2018)].

For both forward and inverse modeling, the toolbox Brainstorm May 2019 was used in MATLAB R2018a in order to reconstruct the sources from the sensor level EEG signals [Tadel et al. (2011)].

3.6.1.1 Forward modeling

For the forward modeling approach, the location and orientation of current dipoles needs to be defined in order to explain the cortical sources relation to the EEG sensors. This is done on a voxel grid space resembling an approximation of the cortical space. This set of dipoles are called the source space. During the forward modeling the source space is constrained to the cortex and with current dipoles orientated perpendicular to the cortex assigned to 15000 verticies using a default generic head model from Brainstorm for all subjects [Tadel et al. (2011)]. In order to relate the source space to the sensor space, eg. sensor EEG time series signals, the different head tissues must be defined in order to make it possible to solve estimate the current dipole potentials generated in the cortex. This is where the forward problem must be solved. In order to solve this, the symmetric boundary element method (OpenMEEG BEM) was used to calculate the head model in Brainstorm May 2019. This model uses a three layer compartment with the compartments, scalp, skull and brain, where each of these tissues conductivities need to be defined. These values where defined by [Lin & Scott (2012)] and assigned according to their study, with the following values for scalp = 1, Skull = 0.0125 and Brain = 1. The forward model was calculated after defining and locating the 62 electrode locations on the scalp. Locations of the electrode was defined according to the 10-20 electrode placement system as in 3.2.1, and is illustrated in figure 3.6, (2). With the defined head model the forward problem is described by the following equation:

$$V = G \cdot J + n \tag{3.4}$$

In equation 3.4 V describes the measurement matrix in relation to the number of electrodes and time samples, which is [62x31744] from the preprocessed data, illustrated in figure 3.6. G is a lead field matrix, which is compromising of the recorded channels and the time varying current dipole source, which has the dimensions of [62x15000], defined by the number of electrodes and verticies. J describes the magnitude of the dipole sources and n is a noise matrix [Im (2018)].

With the forward problem defined, it is now possible to estimate how the cortex sources determine the values in relation to the EEG sensors obtained from the scalp.For this solution the inverse problem must be solved in order to achieve the the EEG sources, eg.

how the sources of the defined dipoles are estimated in relation to the EEG sensor level recordings.

3.6.1.2 Inverse modeling

In the inverse problem, the activity from the 62 EEG sensors needs to be estimated from the defined dipoles in the forward model, hence the inverse problem is defined from the forward problem, equation 3.4, as:

$$\hat{J} = M \cdot V \tag{3.5}$$

Here $\hat{J}$ is the sources which are being estimated and M is the inverse operator. The inverse problem is an ill posted problem as the number of estimated sources are greater compared to the number of electrodes from the EEG sensor recordings. In order to achieve a solution for this problem, the method of minimum-norm solution is utilized by applying a linear kernel in the form of a matrix that multiplies the spatial data at each point in time. This method estimates cortical current source densities which fits approximately to the data of the forward model, by minimizing overall power of the activity from the estimated sources [Im (2018)]. An ill posedness problem can cause hassles, as a unique solution might not exist for all data [Tadel et al. (2011)]. This is delt with by introducing a prior in the form of a noise covariance matrix, which is an identity matrix assuming equal noise from all EEG sensors, as previously done by [Lai et al. (2018)].

The result of the minimum norm estimate is represented as a current density map, which is the currents found for each point current dipole, in the unit of ampere per meter. The minimum norm estimate have a drawback as it tends to place source activity in superficial regions of the cortex, resulting in a drop in resolution of deeper tissues of the cortex [Tadel et al. (2011), Pascual-Marqui (2002)]. Normalization of the current density map is therefore applied in order to improve localization of the deep sources, using a normalization methods of standardized LOw Resolution brain Electromagnetic TomograAphy (sLORETA), which has shown to have good localization, with small error. sLORETA works by normalizing the current density power at each data point by adding the theoretical signal covariance added to the the the noise covariance [Pascual-Marqui (2002)].

With sources constrained with dipole orientation perpendicular to the cortex, the sources are now represented as normalized current densities perpendicular to the cortex. The number of reconstructed sources are of very high resolution and would be inefficient to calculate functional connectivity from. Therefore a technique of clustering the sources based on a pre-defied atlas with regions of interest (ROIs) on the cortex surface are utilized. In order to define these ROIs a predefined atlas named the Desikan Killiany atlas is used, which defines 68 ROIs on the cortex surface. The regions on the cortex of

the Desikan Killiany atlas can be found in appendix E The sources were clustered as the average time series within the pre-defined ROIs [Tadel et al. (2011), Hassan & Wendling (2018)]. Before averaging the sign of the dipoles with opposite direction were flipped, in order to avoid cancellation of activity because of opposite direction of dipole sources [Hassan & Wendling (2018), Lai et al. (2018)]. With the clustered source time series, the matrix becomes [ROIs x time]. This matrix will be used in the further analysis to calculate the functional connectivity.

3.7 Functional connectivity analysis

For the further analysis of functional connectivity, 60 seconds of artifact free signal were selected from all data sets [Jin et al. (2011)]. Both measures for functional connectivity, MI and PLI were being computed on the source reconstructed EEG signals. MU is a non-direced, information based method for estimating functional connectivity based on the amplitude of the signal, while PLI is a non-directed data driven method based on the phase difference between signals [Im (2018)]. Only PLI accounts for the effects of volume conduction [Im (2018), Ramanand et al. (2011)]

Before the calculation of MI and PLI, the data was divided into narrow band signals. As mentioned in section 3.2.2 physiological interpretation of the signals in the brain can be divided into different frequency bands of different physiological meaning. A 4'th order butterworth filter was used in order to acquire the three frequency bands, Alpha, Beta and Gamma. As the consistency between studies are not consistent in the definition of the frequency ranges, the values where chosen on behalf of the study by [Newson & Thiagarajan (2019)], who defined frequency bands of oscillatory waves of the brain from the most used ranges reported among studies, with the following values, Alpha (7.5-12.5 Hz), Beta (12.5-30 Hz) and Gamma (30-40 Hz).

3.7.1 Mutual Information

Mutual information expresses the shared information between two signals based on Shannon entropy, which is the average amount of information that is needed in order to encode a discrete variable [Im (2018)].

Entropy of a discrete variable X is calculated as:

$$H(X) = -\sum_{x} p(x)\, log\, p(x) \tag{3.6}$$

Here entropy is calculated as the uncertainty of variable X being within the probability distribution of observed variables. Here, $p(x)$ in the formula is the likelihood of the variable x being within the probability distribution of observed variables.

When two variables are being considered, this is denoted the joint entropy and is calculated

as:

$$H(X,Y) = -\sum_{x;y} p(x,y)\, log(p(x,y)) \tag{3.7}$$

Uncertainty within variables X and Y together is being considered here and the probability of these variables existing in the same probability distribution.

Mutual information uses the idea of entropy in order to estimate the amount of shared information which lies between two variables, which is the idea of how much information variable X contains about variable Y, and visa versa. Mutual information is consequently calculated as:

$$I(X;Y) = \sum_{x}\sum_{y} P(x,y)\, log\frac{P(x,y)}{P(x)P(y)} \tag{3.8}$$

The dependence between variables are expressed through MI. A greater value is correlated with higher dependence between the variables. MI only gives values that are equal to or higher than zero, zero meaning total independence between variables, but only if the variables are statistically independent. MI accounts for both linear and non-linear dependencies [Batina et al. (2010), Wang et al. (2010)].

MI was computed between every electrode. To do this, firstly the probability distribution of signals sY and sY were defined:

$$P_{sX,sY}(i,j) = \frac{b(i,j)}{N} \tag{3.9}$$

The number of observations per bin in the histogram defining the joint probability distribution of sX and sY is defined as $b(i,j)$ and N is the amount of samples used [Bingham et al. (2017)]. In order to estimate the number of bins represented in the histogram, the following equation was used [Rosenblum et al. (2001)]:

$$N_{bins} = exp(0.626 + 0.4 * log(N-1)) \tag{3.10}$$

For the computation of the MI from the EEG signals, entropy of signal X and Y were estimated by the probability distribution 3.9 and the MI were then calculated from equation 3.8.

As MI has shown to give rise to more errors when calculated over small sample counts and calculation of MI over epochs of longer sample lengths has shown greater Gaussian distribution characteristics [Roulston (1999), Wang et al. (2009), Sazonov et al. (2009)], MI were therefore calculated over four second non-overlapping epochs, which was equivalent to 2048 samples. This gave a bin size of 40 from equation 3.10. The size of the bins were defined from the possible data range, from the lowest to the highest value within the dataset, in order to keep equal bin size. The range of the data can be found in D. After the computation of MI between every two channels in a pair, the MI computed for each four second epoch were averaged to give one value representing the MI value per channel dependence.

3.7.2 Phase Lag Index

PLI quantifies the asymmetry of the distribution of differences in instantaneous phase, either positive or negative differences, between two signals, if non zero phase lag are present between the two signals. Non zero phase difference between the signals are implied for, in the asymmetry, in case the phase synchronization is caused by common sources[Im (2018)].

In order to estimate PLI, the phase information must be calculated from the signals of interest. This can be achieved by the Hilbert transform [Siuly et al. (2016), Seraj (2018), Im (2018)] The Hilbert transforms of a signal $x(t)$ can be simply explained as a shift in phase from the original signal by $\frac{\pi}{2}$ for positive frequencies and $-\frac{\pi}{2}$ for negative frequencies and is defined as:

$$Hx(t) = \frac{1}{\pi} PV \int_{-\infty}^{\infty} \frac{x(\tau)}{t-\tau} d\tau \tag{3.11}$$

Because of a potential singularity at t=τ, the integral in the Hilbert transform is calculated by means of the Cauchy Principal value PV [Seraj (2018)] In order to calculate the phase of the signal, the analytic signals must be defined, this can be done as:

$$Z(t) = A(t)e^{j\phi(t)} \tag{3.12}$$

A(t) is defining the instantaneous amplitude, while ϕ defines the instantaneous phase [Seraj (2018), Colclough et al. (2016), Stam et al. (2007)]. The phase information can then be extracted using the Hilbert transform:

$$\phi(t) = arctan \frac{Hx(t)}{x(t)} \tag{3.13}$$

The PLI between two signals can then be calculated from the average phase difference between two signals $x(t)$ and $y(t)$ using equation Fraga González et al. (2018). The *sign* determines if the phase difference is positive, negative or zero value [Im (2018)].

$$PLI_{x,y} = \left| \frac{1}{N} \sum_{t=1}^{N} sign[sin((\phi_x(t) - \phi_y(t))] \right| \tag{3.14}$$

The computation of PLI were done between every two channels in a pair from the EEG signals, by first computing the analytic signal from equation 3.12, where after the phase of the signals where calculated by equation 3.13, in order to calculate the PLI from equation 3.14. The result of the computed PLI lies in the interval from zero to one, where one means that there is no coupling between the two signals, and the signals is most likely within the interval of less than 0< phase difference <ϕ and one indicated as perfect coupling between the signals. PLI were calculated over epoch of lengths similar for MI computations, 4 second epochs, equivalent to 2048 samples, in order to keep consistency.The PLI data were stored in s similar adjacency matrix of dimension $NcxNr$, with zeros along the diagonal.

3.8 Statistics

As the EEG signals are composed of multi-channel data, a problem arises in the form of the multiple comparison problem (MCP), as the family wise error (FWER) are not being controlled. With many comparisons the risk of making a type one error increases, thus giving rise to poor interpretation of the results. One solution of controlling the FWER is by Bonferroni correction, but this method increases the risk of making a type two error, thus being very conservative, lowering the power of the statistical test [De Leon & Fernandez Donoso (2017)]. For this reason the less conservative method cluster based permutation test are the used for comparing the data within and between subjects [Huang & Zhang (2017)]. For the statical test the source reconstructed EEG signals were divided into the three frequency bands Alpha, Beta and Gamma, prior to calculating the functional connectivity metrics [Lai et al. (2018), Kabbara et al. (2017)]. Linear regression analysis were used to asses the relationship between results obtained from PLI and MI metrics.

3.8.1 Non-parametric cluster based permutation test

The non-parametric cluster based permutation test were computed using MATLAB 2018a, utilizing the toolbox FieldTrip developed at Donders Institute, Brain, Cognition and Behavior, Nijmegen in the Netherlands, by researchers .

Non-parametric cluster based statistical test is a method to do statistical testing while controlling the FWER [Maris & Oostenveld (2007)]. The basic idea of the non-parametric cluster based permuation test is to construct a histogram of the test statistic through permutation of the samples, resembling a non parametric estimate of the probability distribution for the test statistic. This distribution is then used to asses p-values in order to reject the null hypothesis. It is possible to choose the test statistic for specific applications and different information. For this project clustering in space are the chosen approach of cluster statistic as the adjacency matrices resembles the connectivity between brain regions. This cluster statistic t_m is used as test static by clustering in the form of summed pixels tm for a specific amount of clusters with p_m amounts of pixels contained in each cluster [Hald (2017)], defined by:

$$t_m = \sum_{i=1}^{p_m} t_i \tag{3.15}$$

The histogram for the test statistics were calculated using Monte Carlo sampling with 5000 permutations at a significance level of 0.5. The t-values which exceeds the critical t-value corresponding to the alpha-level of 0.05, were being clustered in sets dependent on their adjacency. The biggest clustered t-value in each round, calculated from 3.7, were assigned to the permutation distribution of test statistics. The p-values were then assessed to find cluster level statistics in the observed data which exceed the threshold of the critical level of the constructed permutation distribution, which are then considered statistically significant [Huang & Zhang (2017)]. Figure 3.7 illustrates an example of the

assessment of significant clusters in the observed data, to give a better understanding of the test. In the figure both the permutation test critical value, corrected by clustering and uncorrected critical value are displayed to give an idea of how the FWER is controlled.

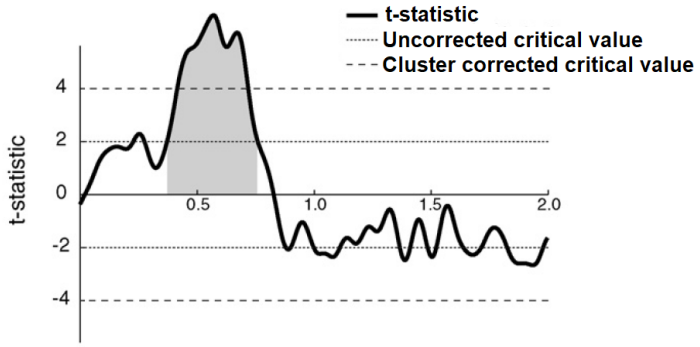

Figure 3.7: Illustration of the assessment of the significance of the observed data, assessed from permutation testing. In the figure one observed cluster are observed to exceed the critical value of the permutation distribution, while many significant data points are observed in case the critical value is not corrected [Maris & Oostenveld (2007)]

Prior to the cluster based permutation test the adjacency matrices where thresholded to only show 20% of the strongest connections, as the strongest connectivity counts have been shown to reflect greater information of the underlying network architecture [Ming et al. (2018)]. Furthermore the well studied resting state network, the DMN were derived from the adjacency matrices, only considering brain regions within the network [Kabbara et al. (2017)]. The cluster based permutation test where then computed to look for differences within the whole brain connectivity and DMN connectivity, which respectively corresponded to the full adjacency of 68x68 brain regions and DMN adjacency matrices of 14x14 brain regions. For the DMN analysis only regions of the brain considered within the DMN were included . This yielded a 14x14 matrix. [Van Den Heuvel & Pol (2011), Kabbara et al. (2017), Dunkley et al. (2018)] In appendix A a list of the brain regions contained in the whole brain adjacency matrices and DMN matrices ae shown.

3.8.2 Linear regression analysis

In order to view the relationship between the two connectivity metrics MI and PLI, a linear regression analysis were performed. Linear regression is a statistical model considering the relationship between two variables X and Y [Asuero et al. (2006), Miller (2013)] The model can be expressed as:

$$Y = \alpha + \beta X + \epsilon \tag{3.16}$$

In equation 3.16 X is a independent variable and Y is a dependent variable. Both α and β are constants, while ϵ is a term of random error. A way of computing the relationship between the variables the coefficient of determination can be computed for the linear

regression model, known as R^2. The residual sum of squares (R_{SS}) and the total sum of squares (T_{SS}) can be used for calculating R^2 [Asuero et al. (2006), Miller (2013)]. These are defined as:

$$R_{SS} = \sum_{i=1}^{n} (y_i - \alpha - \beta x_i)^2 \tag{3.17}$$

$$T_{SS} = \sum_{i=1}^{n} (y_i - \bar{Y})^2 \tag{3.18}$$

Where $\bar{Y}$ is the mean of Y, in equation 3.18. The coefficient of determination can now be computed from the following equation:

$$R^2 = 1 - \frac{RSS}{TSS} \tag{3.19}$$

The method explains the amount of total variation in regards to the mean, which is explained by the regression R^2 and results in a computed output value between zero and one, where zero means that there is no relationship between the variables and one meaning that there is a perfect relationship between the variables [Asuero et al. (2006)]. R^2 can also be negative in case of a negative relationship [Miller (2013)]

For the linear regression analysis the data obtained from the control session at the pre stage were used, as it is assumed that the rest of the data will have same trends, as the same methods were applied to all data. Linear regression were computed between PLI and MI at Alpha, Beta and Gamma band.

4 | Results

In this section, the results of the data analysis will be presented.Initially a presentation of the results from the cluster based permutation test will be presented, followed by a network visualization of the significant differences in functional connectivity, showing which brain regions are involved. PLI and MI metrics are compared by linear regression analysis, in order get an objective measure on the similarity in results between the two metrics.

4.1 Cluster based permutation test

The cluster based permutation test were used in order to localize any significant clusters in the connectivity differences between brain regions of the adjacency matrices.

From the whole brain analysis no significant clusters where found at an Alpha level of 0.05. However, the clusters tended to be significant were highlighted when p-value were lower than 0.1, in order to look for trends in the data. A trend were present for the PLI metric within the SM session in the form of Alpha and Gamma oscillatory changes. Also between SM and control sessions changes where seen in the Alpha frequency range. Within the MI metric only a trend within SM Alpha oscillatory changes where present. Within the DMN network, significant clusters where present at the Alpha band frequency range for SM session and between SM and control for the PLI metric at a significance level below 0.05. No significant results or trends where found within the control group. The results of the cluster basted permutation test shown from the adjacency matrices are illustrated in appendix A. Tables 4.1, 4.5 and 4.7, shows an overview of the results from the cluster based permutation test. In the tables, 'SM' denotes the comparison of Pre to Post measurement in the SM session, while 'Ctrl' denotes the comparison of Pre to Post measurement in the control session. These comparisons show if any changes are present within any of the two sessions. 'SM vs. Ctrl' denotes the comparison between SM and control session as the absolute difference from Pre to Post, in order to view how each intervention compare against each other. Positive ($+clusters$) clusters indicates an increase in connectivity while negative clusters ($-clusters$) indicate a decrease. The cluster count is determined from the amount of clusters that exceeded the significance level of the critical t value, $t(23) = \pm 2.0687$, without the FDR correction, with 24-1 degrees of freedom, at the significance level of 0.05.

In order to get a better understanding of the changes found, which are presented in the tables 4.1, 4.5 and 4.7, they are visualized at the cortex level with the connected brain regions and by a circular graph plot. The circular graph plots shows the effect size of the difference in connectivity, while the visualization of the networks in the cortex shows the strength of each brain region (nodes) and connectivity (weighted edges) between these

regions. The edges denotes how each node are interconnected between nodes and vary in size according to their weight. The nodes are represented as the strength of the connectivity within the node and shows how much influence they have in the network. Bigger node size are correlated with a bigger influence in the network. Red nodes corresponds to increase in connectivity, while blue nodes corresponds to a decrease. During explanation of connections between certain brain regions, they will be refereed with the following notation, 'node - metric - node', for easier explanation and reader compliance.

4.1.1 Whole brain functional connectivity

The whole brain connectivity compromised of all brain regions of the 68x68 adjacency matrices. Tended clusters which exceed the permutation distribution threshold at a significance level of 0.1 were highlighted. In the result section this will be represented as circular graph plots and network visualization at the cortex level. The adjacency matrices with highlighted clusters can be found in appendix B, names of the brain regions and their abbreviation are also found in the appendix A and are listed in a table with the order corresponding to the order they are outlined in, in the adjacency matrix, starting from the left upper corner pixel, or lower left corner pixel. Firstly results from the PLI metric will be presented, followed by the MI metric.

4.1.1.1 Phase Lag Index

The cluster based permutation test performed on the whole brain PLI connectivity metric are shown in table 4.1. One cluster is showing a trend in both within SM session and between the SM vs. Ctrl comparison at the Alpha frequency band. A cluster is also present at the Gamma band within the SM session, which exceeds the Alpha level of 0.1.

Table 4.1: Whole brain functional connectivity comparison for PLI. Positive (+) and negative (-) cluster count are shown, with t-value and p-values in case of any significant clusters were present.

p<0.1			If significant			If significant	
		+clusters	**t-value**	**p-value**	*−clusters*	**t-value**	**p-value**
Alpha	Ctrl	136	-	-	98	-	-
	SM	130	-	-	98	-12.66	0.068
	SM vs. Ctrl	114	-	-	134	-12.62	0.074
Alpha	Ctrl	94	-	-	84	-	-
	SM	110	-	-	116	-	-
	SM vs. Ctrl	92	-	-	108	-	-
Gamma	Ctrl	94	-	-	110	-	-
	SM	120	11.97	0.071	90	-	-
	SM vs. Ctrl	94	-	-	94	-	-

From table 4.1 tended clusters were present from the comparison between SM and control session and within the SM session comparison at the Alpha frequency band. Also One

significant cluster is present at the Gamma frequency band within the SM session.

SM - Alpha band

Within the SM session decreased connectivity in the Alpha band were seen in table 4.1 (t=-12.66, p=0.068), this is illustrated by figure 4.1. Here the right insula were mainly driving this decrease. Decreases were seen between 'left insula - PLI - right parahippocampal', 'right insula - PLI - light parahippocampal', 'right insula - PLI - right parahippocampal', 'right insula - PLI - left lingual', 'right insula - PLI - right lingual'.

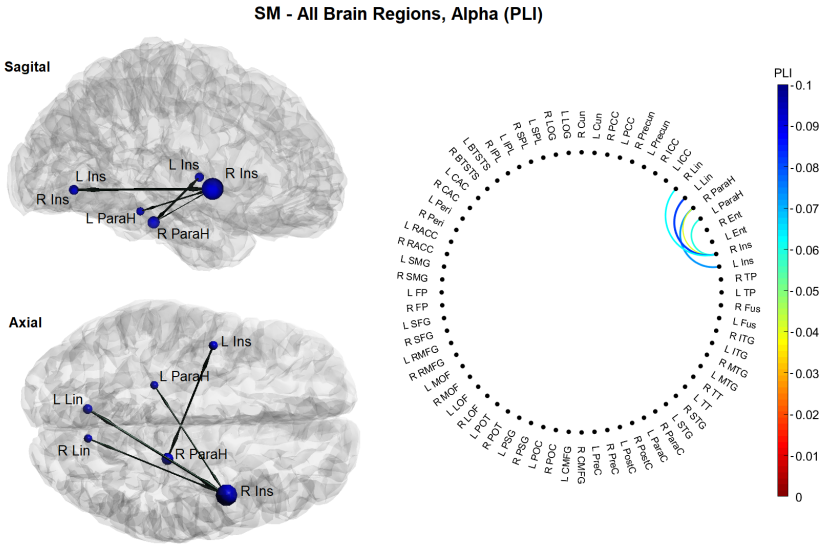

Figure 4.1: Illustration of the connectivity change between brain regions, greater value indicates bigger decrease in PLI in the circular graph, located to the right in the figure. The network visualizes the nodes as blue colors as they decrease in connectivity within the cortex level, located to the left in the figure.

Table 4.2 shows the effect size which were occurring from the connectivity change in figure 4.1.

Table 4.2: Effect size of tended clusters in the whole brain PLI Alpha band comparison, within the SM session

Nodes	**Effect** size
L Ins - PLI - R ParaH	−0.0743
R Ins - PLI - L ParaH	−0.0614
R Ins - PLI - R ParaH	−0.0417
R Ins - PLI - L Lin	−0.0829
R Ins - PLI - R Lin	−0.0638

SM vs. Ctrl - Alpha band

A negative trend in Alpha band functional connectivity change between SM and control

session were seen from table 4.1 by the negative t-value (t=-12.62, p=0.074). The brain regions which were involved in this change are illustrating a decrease in PLI, illustrated in figure 4.2. The involved brain regions that contributes mostly to this decrease were the left inferior parietal lobule and the left caudal middle frontal gyrus. Decreases were seen between 'right pars opercularis - PLI - left inferior parietal lobule', 'left caudal middle frontal gyrus - PLI - right superior partial lobule ', 'left caudal middle frontal gyrus - PLI - left inferior partial lobule', 'left caudal middle frontal gyrus - PLI - right inferior partial lobule', 'right caudal middle frontal gyrus - PLI - left inferior parietal lobule'.

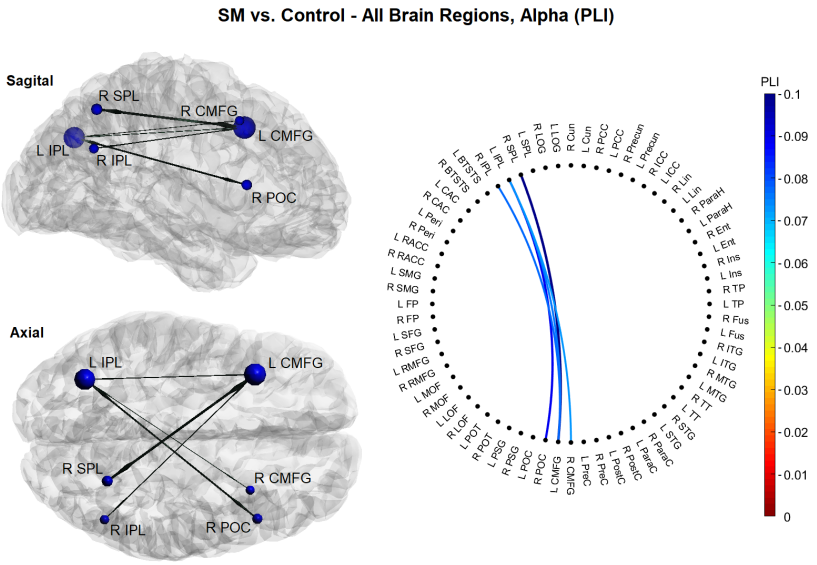

Figure 4.2: Illustration of the connectivity change between brain regions, greater value indicates bigger decrease in PLI in the circular graph, located to the right in the figure. The network visualizes the nodes as blue colors as they decrease in connectivity within the cortex level, located to the left in the figure.

Table 4.3 shows the effect size which were occurring from the connectivity change in figure 4.2.

Table 4.3: Effect size of tended clusters in the whole brain PLI Alpha band comparison, between SM vs. Ctrl

Nodes	Effect size
R POC - PLI - L IPL	−0.0898
L CMFG - PLI - R SPL	−0.1009
L CMFG - PLI - L IPL	−0.0773
L CMFG - PLI - R IPL	−0.0787
R CMFG - PLI - L IPL	−0.0737

SM - Gamma band

Within the Gamma band a trend showed as an increased connectivity in the SM session (t=11.97, p=0.071) within the frontal part of the cortex, illustrated by figure 4.3. Increased connectivity were present between 'left frontal pole - PLI - right frontal pole', 'left frontal pole - PLI - left superior frontal gyrus', 'left frontal pole - PLI right superior frontal gyrus' and 'right frontal pole - PLI - right superior frontal gyrus'.

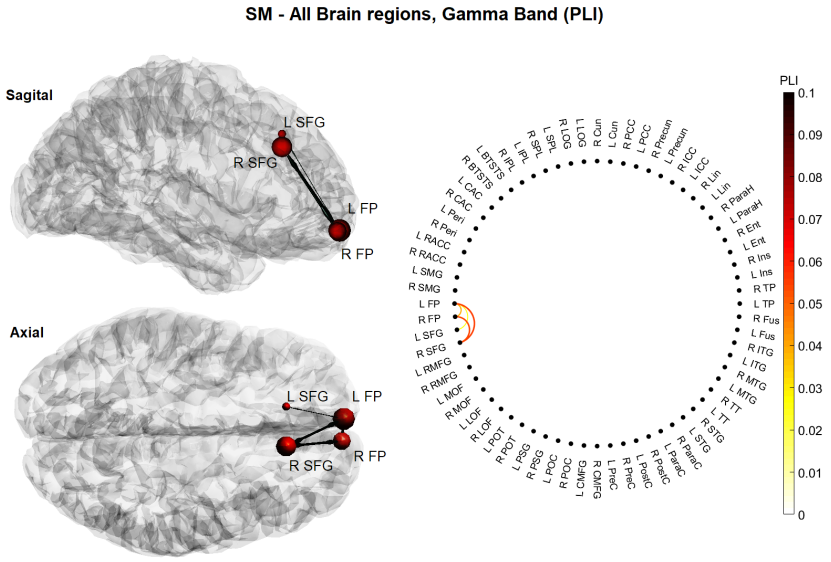

Figure 4.3: Illustration of the connectivity change between brain regions, greater value indicates bigger decrease in PLI in the circular graph, located to the right in the figure. The network visualizes the nodes as red colors as they increase in connectivity within the cortex level, located to the left in the figure.

Table 4.4 shows the effect size which were occurring from the connectivity change in figure 4.3.

Table 4.4: Effect size of tended clusters in the whole brain PLI Gamma band comparison, within the SM session

Nodes	Effect size
L FP - PLI - R FP	0.0399
L FP - PLI - L SFG	0.0281
L FP - PLI - R SFG	0.0562
R FP - PLI - R SFG	0.0551

4.1.1.2 Mutual Information

The cluster based permutation test performed on the MI connectivity metric are shown in table 4.5. One cluster showed a trend from the SM session comparison at the Alpha frequency band, which exceeded the Alpha level of 0.1 were present.

Table 4.5: Whole brain functional connectivity comparison for MI. Positive (+) and negative (-) cluster count are shown, with t-value and p-values in case of any significant clusters were present

p<0.1			If significant			If significant	
		+clusters	**t-value**	**p-value**	*−clusters*	**t-value**	**p-value**
Alpha	Ctrl	44	-	-	24	-	-
	SM	64	-	-	98	-	-
	SM vs. Ctrl	92	-	-	86	-	-
Alpha	Ctrl	44	-	-	58	-	-
	SM	46	9.7700	0.0830	74	-	-
	SM vs. Ctrl	58	-	-	74	-	-
Gamma	Ctrl	38	-	-	54		-
	SM	58	-	-	64	-	-
	SM vs. Ctrl	60	-	-	76	-	-

SM - Alpha band

A trend in the form of an increase within the Alpha band frequency range (t=9.77, p=0.083) are shown in table 4.5. Tended increase were seen between 'left precuneus - MI - left inferior partial lobule', 'right precuneus - MI - right superior partial lobule, 'right precuneus - MI - left partial lobule', 'left posterior cingulate cortex - MI left inferior partial lobule'. These increases are visualized in figure 4.4

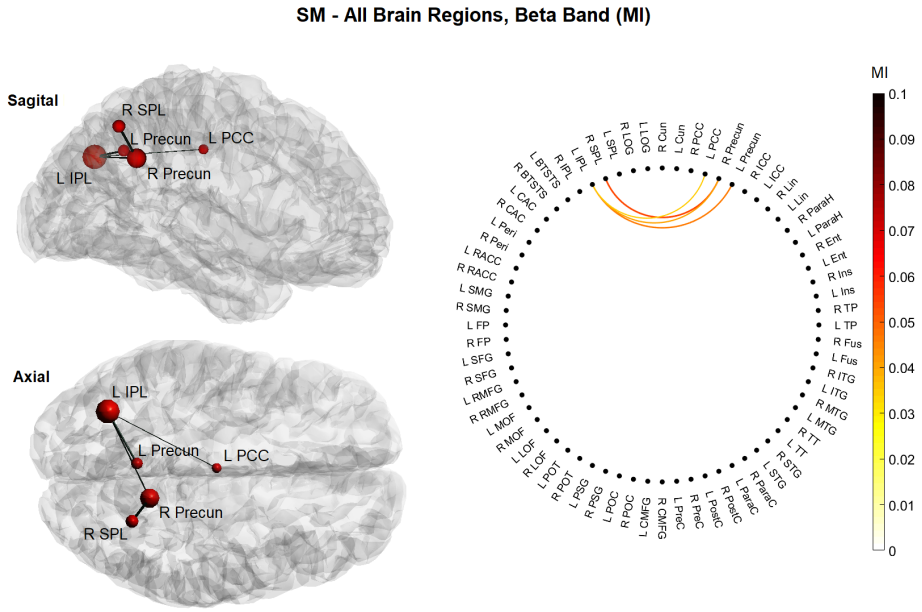

Figure 4.4: Illustration of the connectivity change between brain regions, greater value indicates bigger decrease in MI in the circular graph, located to the right in the figure. The network visualizes the nodes as red colors as they increase in connectivity within the cortex level, located to the left in the figure.

Table 4.6 shows the effect size which were occurring from the connectivity change in figure

4.4.

Table 4.6: Effect size of tended clusters in the whole brain MI Beta band comparison, within the SM session

Nodes	Effect size
L Precun - MI - L IPL	0.0482
R Precun - MI - R SPL	0.0546
R Precun - MI - L IPL	0.0420
L PCC - MI - L IPL	0.0359

4.1.2 Default mode network connectivity

Within the DMN, significant results where seen from the SM session and between SM and control sessions in DMN functional connectivity for the PLI metric at a significance level of 0.05. No significant results where observed in the control group, nor for the MI metric. The significant results are illustrated in table 4.7. Results from the MI metric for the DMN can be found in the appendix C.

Table 4.7: DMN comparison for PLI. Positive (+) and negative (-) cluster count are shown, with t-value and p-values in case of any significant clusters were present

p<0.05			If significant			If significant	
		+ clusters	**t-value**	**p-value**	**- clusters**	**t-value**	**p-value**
Alpha	Ctrl	0	-	-	6	-	-
	SM	8	10.4500	0.0048	6	-	-
	SM vs. Ctrl	6	10.3600	0.0120	0	-	-
Beta	Ctrl	4	-	-	0	-	-
	SM	6	-	-	4	-	-
	SM vs. Ctrl	2	-	-	2	-	-
Gamma	Ctrl	6	-	-	8	-	-
	SM	2	-	-	4	-	-
	SM vs. Ctrl	4	-	-	2	-	-

SM - Alpha band

Figure 4.5 shows the significant cluster found by the cluster based permutation test for the SM session within the DMN (t=10.36, p=0.012). These changes were found as an increase in Alpha band connectivity between nodes of significant size. The involved nodes which exhibit an increased connectivity were found between 'left parahippocampal - PLI - left posterior cingulate cortex', 'left parahippocampal - PLI - right posterior cingulate cortex', 'right parahippocampel - PLI - left posterior cingulate cortex', 'right parahippocampel - PLI - right posterior cingulate cortex'. This difference were greater in the left hemisphere, compared to the right.

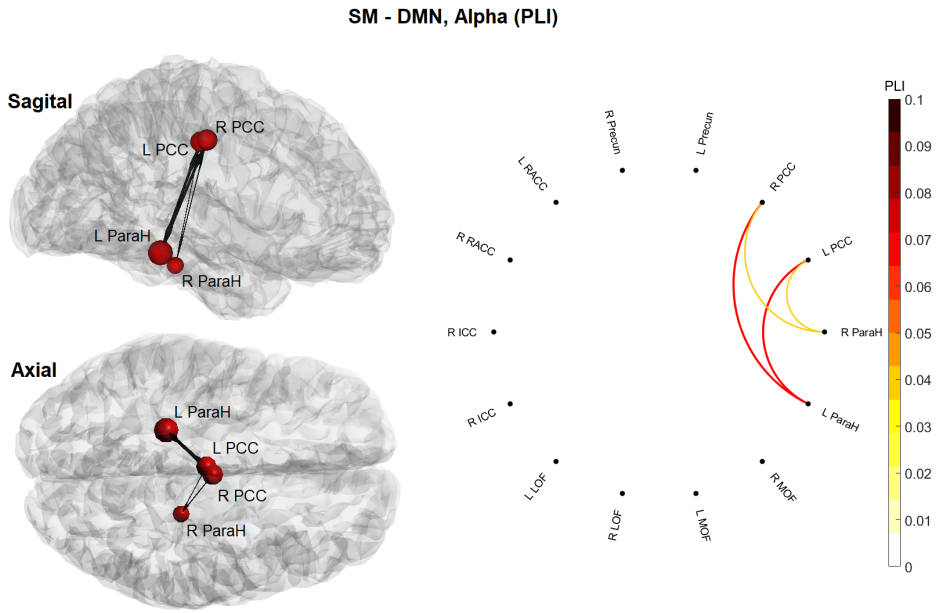

Figure 4.5: Illustration of the connectivity change between brain regions, greater value indicates bigger increase in PLI in the circular graph, located to the right in the figure. The network visualizes the nodes in red as they increase in connectivity.

Table 4.8 shows the effect size which were occurring from the connectivity change in figure 4.5.

Table 4.8: Effect size of significant clusters in DNM PLI Alpha band comparison, within the SM session

Nodes	Effect size
L ParaH - PLI - L PCC	0.0752
L ParaH - PLI - R PCC	0.0755
R ParaH - PLI - L PCC	0.0444
R ParaH - PLI - R PCC	0.0483

SM vs. Ctrl - Alpha band

The significant results from the comparison between SM and control session are illustrated in figure 4.6, (t=10.45, p=0.0048). The same brain regions where involved as in figure 4.5 with an additional difference in increased connectivity between 'left parahippocampel - PLI - right parahippocampel' and loss of a significant difference between 'right parahippocampal - PLI - right posterior cingulate cortex'. The greatest changes present here were increased connectivity between the left parahippocampal regions to the right and left posterior cingulate cortex.

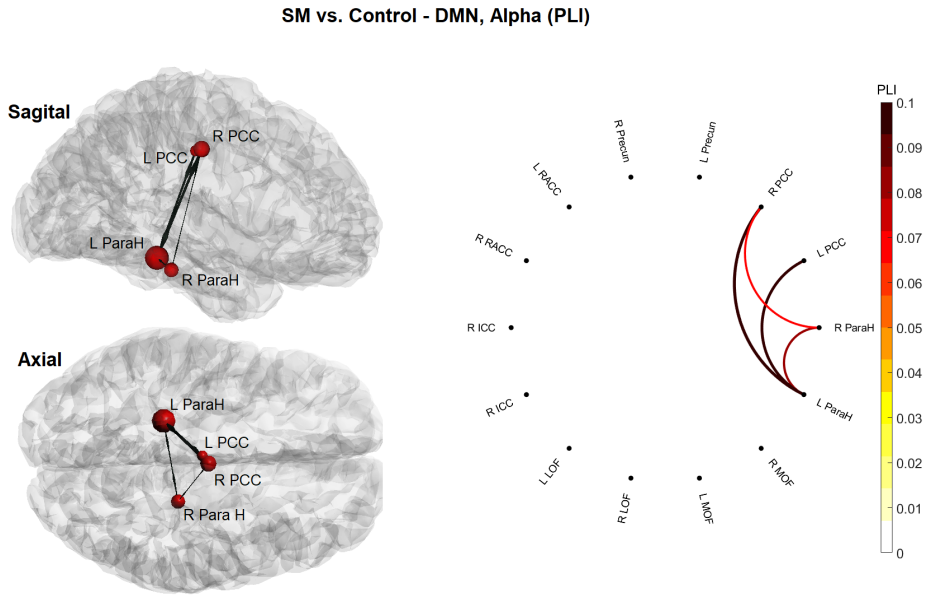

Figure 4.6: Illustration of the connectivity change between brain regions, greater value indicates bigger increase in PLI in the circular graph, located to the right in the figure. The network visualizes the nodes in red as they increase in connectivity.

Table 4.9 shows the effect size which were occurring from the connectivity change in figure 4.6.

Table 4.9: Effect size of significant clusters in DNM PLI Alpha band comparison, between SM vs. Ctrl

Nodes	Effect size
L ParaH - PLI - R ParaH	0.0863
L ParaH - PLI - L PCC	0.1080
L ParaH - PLI - R PCC	0.1179
R ParaH - PLI - R PCC	0.0767

4.2 Metric comparison

From the results shown in the prior section, PLI and MI do not reflect same results. In order to see their relationship in a more objective way, a linear regression analysis were performed between PLI and MI metrics. The signal range for the three frequency bands can be found in appendix D, which where the values uses for the binning during the MI calculations.

Figure 4.7 shows the results from the linear regression analysis between PLI and MI metrics for both Alpha, Beta and Gamma frequency bands. The linear regression analysis were based on the pre control measurements after source reconstruction and frequency

band computation, results can be seen in table 4.10. Figure 4.7 illustrates the results as an example from subject one.

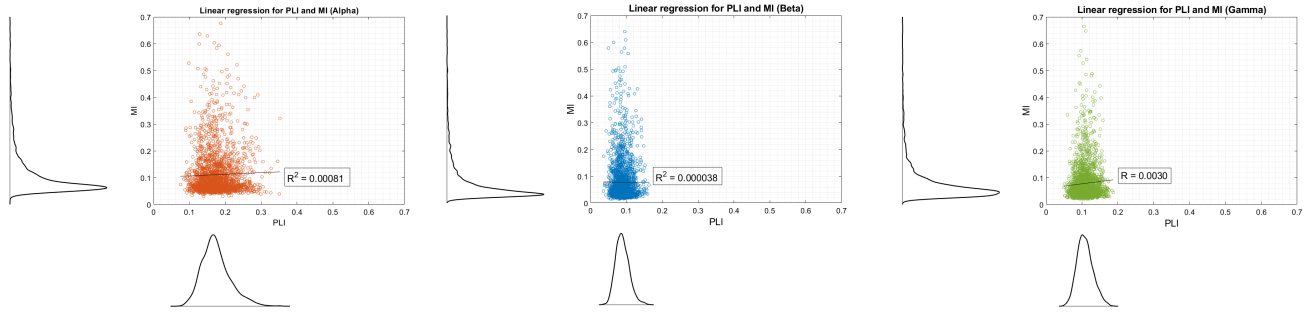

Figure 4.7: Illustration of the linear regression analysis from subject one pre control measurement. The red, blue and green values represent Alpha, Beta and Gamma frequency band respectively. A line is plotted through the data showing the coefficient of determination R^2. The histograms displaying the distribution of the values.

The coefficient of determination R^2 were not reflecting a relationship between PLI and MI in regards to computing the same connectivity values for the data. PLI have a narrower range of values which are considered within the results, while the MI results shows more variation. In order to show the variation within the data and thus between metrics, the median along with the standard deviation are computed over the entire dataset of control session at the pre stage, this is shown in table 4.10. The median are shown as this is more robust for outliers in the data Zomet et al. (2001).

Table 4.10: Median values of pre control measurement, showing median values for the coefficient of determination R^2 and median values for Alpha, Beta and Gamma band

	Median R^2	**Median PLI**	**Median MI**
Alpha	0.0007 ± 0.0071	0.1698 ± 0.0402	0.0832 ± 0.0954
Beta	0.0008 ± 0.0042	0.0837 ± 0.0174	0.0387 ± 0.0780
Gamma	0.0023 ± 0.0027	0.1076 ± 0.0218	0.0391 ± 0.0701

5 | Discussion

From the authors knowledge, this is the first study to address the mechanisms of SM through functional connectivity analysis on resting state EEG data in chronic stroke patients. Significantly increased functional connectivity within nodes of the DMN were found in PLI alpha band between posterior cingulate cortex nodes and parahippocampal nodes within SM session t(23)=10.45, p=0.0048. Similar results where observed in the SM vs. contro comparison, t(23)=10.36, p= 0.012. The discussion will mainly focus on these findings as they are more consistent. The brain regions that where found to have tended differences might be drawn parallels to within the discussion with reference to the figures in these cases. Furthermore PLI and MI expresses no relationship between calculated connectivity results, from the linear regression analysis. This can be caused for several reasons, which will be discussed here.

5.0.1 Increased functional connectivity between brain regions within the DMN

Not many studies address the relationship between manual therapy, like SM, with functional connectivity in the brain, therefore the literature is limited. One study by Gay et al. (2014) that addresses manual therapies role, including SM, on functional connectivity in healthy subjects, shows immediate changes in functional connectivity between certain brain regions, including regions of the DMN, for instance increased connectivity from the posterior cingulate cortex. These findings where found along with a decrease of pain perception following manual therapy. Studies investigating the role of the DMN in stroke patients, have mainly found decreased functional connectivity, compared to healthy subjects [Gay et al. (2014), Li et al. (2014), Baliki et al. (2014), Alshelh et al. (2018)]. This makes default mode activation and connectivity of special interest when examining cognitive dysfunction in psychiatric and neurologic brain disorders [Van Den Heuvel & Pol (2011)]. Stroke has been often shown to lead to chronic pain O'Donnell et al. (2013). SM therapy have been studied in relation to relieving pain and evidence for this method to alter pain threshold exists [Li et al. (2014), Salehi A et al. (2015), Palmgren et al. (2006)]. An altered pain threshold might have been a result of increased functional connectivity from regions of the DMN, during this study, as a result of SM, assumable reflecting relief of pain in the stroke patients [Li et al. (2014)]. Disrupted functional connectivity within the DMN is linked with patients suffering from chronic pain [Alshelh et al. (2018)]. The fact that the specific nodes of the posterior cingulate cortex and parahippocampal showed significant differences, might be caused by the function of these regions to modulate functional connectivity between DMN nodes. The posterior cingulate cortex is one of the major regions within the DMN and the connectivity between this and the parahipocampal has been shown to link the hippocampus with the medial temporal lobe [Karafin et al. (2016)]. Reduction of functional connectivity between these regions have been found to be involved in pain modulation and the development of chronic pain syn-

drome via functions that are implicated in chronic pain, including introspection, emotion and memory. Altered dynamics of the DMN is therefore believed to be part of chronic pain development [Karafin et al. (2016), Ward et al. (2013)]. These changes can be seen as maladaptive neuroplasticity of the adult brain caused by a disease, showing as a loss in functional connectivity within the DMN [Karafin et al. (2016)]. The cause of this decrease in connectivity can be explained from the DMNs activation responsibility for non task related work. In the healthy brain the DMN is one of the essential networks that are activated during rest and deactivated during task related work. Disruptions during rest within this network is linked with neorulogic diseases like stroke [Smith et al. (2018*a*)]. One explanation of the decreased DMN connectivity can be postulated by the fact that the brain of chronic pain patients never fully rest, as the pain perception is involved in the background activity of the brain during rest in these patients, while in healthy patients regions of the DMN shows higher connectivity during rest, as this network is believed to reflect mind attention, memory, self processing and proseption [Baliki et al. (2008), Alshelh et al. (2018)]. If counter intuitive emerging stimuli, not related to the normal function of the DMN at rest demonstrates absence of a task, the brain is not at full rest because it processes this information. Because the perception of pain is not being coupled with noxious stimuli, thus it is linked to background functions, which is also present at rest. Introspection and memory are thought to play a role in the pathogenesis of chronic pain [Karafin et al. (2016)]. Furthermore increased insular cortex connectivity have been found to increase with pain intensity [Baliki et al. (2014)]. The tended decreases in the SM group in figure 4.1 might reflect this as a decrease in the pain perception, while the nodes within the DMN network increased, which controversially has been show to decrease in chronic pain patients [Baliki et al. (2014)].The fact that this change happens in the alpha band makes sense, as this frequency band reflects brain activity of relaxed state as mentioned in section 3.2.2.

As it is unknown whether the subjects in this study were in pain at the time of the study, nor whether this changed after SM, changes in pain perception may not be the only explanation of the results of this study. As mentioned, the current study has shown that SM in a chronic stroke patients increased functional connectivity between the posterior cingulate cortex and the parahippocampal regions within the DMN in alpha band connectivity. These results could also reflect improved cognitive function, such as improved episodic memory following SM. Abnormal connectivity in the posterior cingulate cortex and hippocampus has been identified in early Alzheimer's disease and mild cognitive impairment patients. Reductions in connectivity from both the posterior cingulate cortex and hippocampus to the wider brain as well as between these two regions are thought to be primary factors in episodic memory impairment associated with early Alzheimer's disease Zhou et al. (2008). It is therefore possible that the increased connectivity found after spinal manipulation in the current study reflects improved episodic memory for the stroke patients. Also both imaging and animal experiments link especially the posterior cingulate cortex and hippocampus parts of the DMN to spatial representation and navigation, which might have been altered following SM [Smith et al. (2018*b*)].

Future studies are needed in order to see whether SM leads to altered chronic pain perception, cognitive improvements and improved spatial navigation in this population, which might be indicated in this study.

5.0.2 Poor relationship between PLI and MI metrics

From the linear regression analysis the PLI and MI metrics did not show high correlation from the calculated connectivity measures, which presumably wouldn't be expected either. There can be several explanations for the missing relationship between these metrics. MI shows greater variability within the computed connectivity data, which might be caused by non robustness to field spread. Estimation of functional connectivity within the sensor level suffers from volume conduction as mentioned in section 3.5, but even in the source level from solving the inverse problem trivial spatial correlations still exists, decreasing with distance and affected by the sampling density [Liu et al. (2018), Colclough et al. (2016)]. For this reason it is recommended to use connectivity measures that accounts for field spread and are robust against this [Colclough et al. (2016)]. This might explain the high values within MI estimates, as this metric doesn't account for zero lag correlations. The drawback of using measures that account for field spread is that they are less consistent, compared to methods which doesn't [Colclough et al. (2016)]. MI is an estimation of shared information between two signals from their marginal probability distributions and the entropy, as a statistical measure of dependence, based on the signals amplitude values. The PLI is a measure of phase synchronization, which measures the similarity in the two signals phase angle, by looking at the instantaneous phase difference of the two signals, not accounting for the amplitude. These two approaches can implicate differences in the estimated values.

The shape of the probability distribution during MI computation are highly affected from the method of quantization of the data with respect to bin number and size. The optimal number of bins where estimated from equation 3.10 in section 3.7.1. The bin size of the histograms making up the probability distributions was set in regards to the possible data range within the collected data, D. If bins are big, information can be lost and MI is not estimated properly, on the other hand, if the bins are small, extreme bins might be populated sparsely, which creates an unreliable probability distribution [Legg et al. (2007)]. This might mean that MI could be overestimating in case of smaller amplitude values. There are also suggestions that there the different functional connectivity metric methods simply find different characteristics of physiological meaning within the signals of information, which also could be a reason for difference between them [Colclough et al. (2016)].

5.0.3 Limitations and future work

Several limitations of the study should be considered within the study design and analysis of the result. As the analyzed data is from resting state EEG signals, it can only provide

information about the underlying resting state organization of functional connectivity between brain regions. It should also be kept in mind that resting state data are more abstract to interpret as there is no specific goal for the subject or hypothesis to be investigated, thus this study is more for exploratory purposes. A more direct approach would be to look into specific task related experiments which would imply subjects to improve in a specific task or give information about pain states, which would make comparison of functional connectivity in relation to performance or decreased pain perception possible, and therefore make for a more direct and clear concussion. This would also give a more clear picture on the effects and implications of SM and its clinical use in rehabilitation for stroke patients. The results found from this study are still meaningful as they are among the fist to show that SM likely have some effects on functional connectivity in the brain of chronic stroke patients. It should thus be kept in mind that the found changes in this study are fairly small and it is questionable if it is enough to make a significant difference in relation to rehabilitation of stroke patients. Despite this study showing that the instantaneous effects of SM are small, the long term effects are still unexplored, and would be relevant to prove, as these effects would have more implications in a rehabilitation program. Also the tested patients are chronic stroke patients with different durations of stroke. In case of SM for utilization in rehabilitation of stroke, an intervention might benefit in the early stages of stroke rather than at the chronic stage, in order to get the potential full outcome of the treatment during rehabilitation, as neuroplasticity is maximized here, mentioned in section 2.2. From the findings in this study, these benefits would likely be in the form of a pain relief of post stroke pain, which approximately 10.6 % of all post stroke patients suffers from and has been shown to impair optimal outcome and participation of rehabilitation, thus affecting future quality of life for those patients [Treister et al. (2017)].

The experimental group of participants consisted of a very broad range of stoke sufferers with different lesion site within the hemisphere, either right and left. Thus this study gives a very general overview of changes that happens in the brain, not taking into account for stroke location. Other analysis of the results could be dividing the subjects into right and left hemispheric stroke, which would lead to a more specific analysis in regards to the actual lesion [Liu et al. (2015)]. Another problem in regards of subject variance related to the anatomy is the forward modeling of the head and dipole locations, which might not be precise with the generalized head model, which were used for all subjects in order to solve the forward model in order to do the source reconstruction [Liu et al. (2018)]. This may likely have caused some imprecise dipole location estimates of the different regions of the brain, which would yield for some unreliable comparison. But the method of using a generalized head model when each individual anatomy is unknown, are the best option and have been used by other studies for estimating source level EEG, and sampling density has been shown to have more influence on forward modeling than precision of the head model [Lai et al. (2018), Liu et al. (2018)].

6 | Conclusion

The aim of this study was to explore the effects of chiropractic SM by utilizing the method of MI and PLI to estimate resting state EEG functional brain connectivity, in chronic stroke patients. Through the analysis of the results altered resting state functional connectivity following single session chiropractic SM treatment was found in chronic stroke patients during this study. These changes where only significant within the DMN, and showed as an increased functional connectivity between the posterior cingulate cortex and parahippocampal, which has previously been found to be an important link within the DMN in relation to chronic pain modulation. This increased connectivity might therefore alter information within the brain that processes chronic pain, episodic memory and spatial representation and navigation. Though it is difficult to draw clear conclusiveness to these effects, as these parameters where not included in the study. The mechanisms of SM in stroke patients are therefore uncertain, as it is unknown, thus further research are needed, preferably collecting additional data from the participants in order to gain more specific and robust results and insights into the mechanisms and effects of SM in stroke patients. Though these findings provided by this study are still valid in proving that SM does have an effect promoting neurophysiological changes within the brain of chronic stroke patients. Furthermore the study show that there is a poor relationship between PLI and MI when calculating functional connectivity, even on source reconstructed EEG signal, which should handle the effects of volume conduction.

Bibliography

1. Aagaard, P., Simonsen, E. B., Andersen, J. L., Magnusson, P. & Dyhre-Poulsen, P. (2002), 'Neural adaptation to resistance training: changes in evoked V-wave and H-reflex responses', *Journal of Applied Physiology* **92**(6), 2309–2318.

2. Alia, C., Spalletti, C., Lai, S., Panarese, A., Lamola, G., Bertolucci, F., Vallone, F., Di Garbo, A., Chisari, C., Micera, S. & Caleo, M. (2017), 'Neuroplastic Changes Following Brain Ischemia and their Contribution to Stroke Recovery: Novel Approaches in Neurorehabilitation', *Frontiers in Cellular Neuroscience* **11**(March), 1–22.
URL: *http://journal.frontiersin.org/article/10.3389/fncel.2017.00076/full*

3. Alshelh, Z., Marciszewski, K. K., Akhter, R., Di Pietro, F., Mills, E. P., Vickers, E. R., Peck, C. C., Murray, G. M. & Henderson, L. A. (2018), 'Disruption of default mode network dynamics in acute and chronic pain states', *NeuroImage: Clinical* **17**(October 2017), 222–231.

4. Asuero, A. G., Sayago, A. & Gonz, A. G. (2006), 'The Correlation Coefficient : An Overview', (10), 41–59.

5. Augustine, G. J., Chikaraishi, D. M., Ehlers, M. D., Einstein, G., Fitzpatrick, D., Hall, W. C., Jarvis, E., Katz, L. C., Kauer, J., LaMantia, A.-S., McNamara, J. O., Moonet, R. D., Nicolelis, M. A. L., Purves, D., Reinhart, P. H., Simon, S. A., Skene, J. H. P., Voyvodic, J., White, L. E. & Williams, S. M. (2004), *NeuroScience*, third edit edn, Sunderland, Massachusetts U.S.A.
URL: *https://www.ncbi.nlm.nih.gov/books/NBK10799/*

6. Baliki, M. N., Geha, P. Y., Apkarian, A. V. & Chialvo, D. R. (2008), 'Beyond Feeling: Chronic Pain Hurts the Brain, Disrupting the Default-Mode Network Dynamics', *Journal of Neuroscience* **28**(6), 1398–1403.

7. Baliki, M. N., Mansour, A. R., Baria, A. T. & Apkarian, A. V. (2014), 'Functional reorganization of the default mode network across chronic pain conditions', *PLoS ONE* **9**(9).

8. Batina, L., Gierlichs, B., Prouff, E., Rivain, M., Standaert, F.-X. & Veyrat-Charvillon, N. (2010), 'Mutual Information Analysis: a Comprehensive Study', *Journal of Cryptology* **24**(2), 269–291.

9. Bigdely-Shamlo, N., Mullen, T., Kothe, C., Su, K.-M. & Robbins, K. A. (2015), 'The PREP pipeline: standardized preprocessing for large-scale EEG analysis', *Frontiers in Neuroinformatics* **9**(June), 1–20.

10. Bingham, A., Arjunan, S. P., Jelfs, B. & Kumar, D. K. (2017), 'Normalised mutual information of high-density surface electromyography during muscle fatigue', *Entropy* **19**(12), 1–14.

11. Blum, C. L. (2002), 'Role of chiropractic and sacro-occipital technique in asthma treatment', *Journal of Chiropractic Medicine* **1**(1), 16–22.

12. Brody, H., Grayson, M., Owens, B. & York, A. (2014), 'Stroke', *NatureOutlook* **510**(7506), 1.

13. Cauraugh, J. H., Naik, S. K., Lodha, N., Coombes, S. A. & Summers, J. J. (2011), 'Long-term rehabilitation for chronic stroke arm movements: A randomized controlled trial', *Clinical Rehabilitation* **25**(12), 1086–1096.

14. Chang, Y., Yang, D. & Guo, Y. (2018), 'Surface & Coatings Technology Laser ultrasonic damage detection in coating-substrate structure via Pearson correlation coe ffi cient', *Surface & Coatings Technology* **353**(April), 339–345.

15. Chen, Y.-l., Fan, Y.-t., Liu, H.-l., Wu, C.-y., Wai, Y.-y. & Lin, K.-c. (2015), 'Neuroplastic changes in resting-state functional connectivity after stroke rehabilitation', *Frontiers in Human Neuroscience* **9**(October), 1–12.

16. Christiansen, T. L., Niazi, I. K., Holt, K., Nedergaard, R. W., Duehr, J., Allen, K., Marshall, P., Türker, K. S., Hartvigsen, J. & Haavik, H. (2018), 'The effects of a single session of spinal manipulation on strength and cortical drive in athletes', *European Journal of Applied Physiology* **118**(4), 737–749.

17. Colclough, G. L., Woolrich, M. W., Tewarie, P. K., Brookes, M. J., Quinn, A. J. & Smith, S. M. (2016), 'How reliable are MEG resting-state connectivity metrics?', *NeuroImage* **138**, 284–293.

18. Cutmore, T. R. & James, D. A. (1999), 'Identifying and reducing noise in psychophysiological recordings', *International Journal of Psychophysiology* **32**(2), 129–150.

19. Dalgas, U., Stenager, E., Lund, C., Rasmussen, C., Petersen, T., Sørensen, H., Ingemann-Hansen, T. & Overgaard, K. (2013), 'Neural drive increases following resistance training in patients with multiple sclerosis', *Journal of Neurology* **260**(7), 1822–1832.

20. De Leon, I. & Fernandez Donoso, J. (2017), 'Sharing IP Strategy: Commercialization', *Innovation, Startups and Intellectual Property Management* **56**(4), 45–60.

21. Dunkley, B. T., Urban, K., Da Costa, L., Wong, S. M., Pang, E. W. & Taylor, M. J. (2018), 'Default mode network oscillatory coupling is increased following concussion', *Frontiers in Neurology* **9**(APR).

22. Endres, M., Engelhardt, B., Koistinaho, J., Lindvall, O., Meairs, S., Mohr, J. P., Planas, A., Rothwell, N., Schwaninger, M., Schwab, M. E., Vivien, D., Wieloch, T. & Dirnagl, U. (2008), 'Improving outcome after stroke: Overcoming the translational roadblock', *Cerebrovascular Diseases* **25**(3), 268–278.

23. et. al. Martini, F. H. (2012), *Fundamentals of Anatomy and Physiology*.

24. Fraga González, G., Smit, D. J. A., van der Molen, M. J. W., Tijms, J., Stam, C. J., de Geus, E. J. C. & van der Molen, M. W. (2018), 'EEG Resting State Functional Connectivity in Adult Dyslexics Using Phase Lag Index and Graph Analysis', *Frontiers in Human Neuroscience* **12**(August), 1–12.

25. Fritz, J. M., Koppenhaver, S. L., Kawchuk, G. N., Teyhen, D. S., Hebert, J. J. & Childs, J. D. (2011), 'Preliminary investigation of the mechanisms underlying the effects of manipulation: Exploration of a multivariate model including spinal stiffness, multifidus recruitment, and clinical findings', *Spine* **36**(21), 1772–1781.

26. Gay, C. W., Robinson, M. E., George, S. Z., Associate Professor, P., Perlstein, W. M., Professor, A., Health Scientist, R. & Bishop, M. D. (2014), 'Immediate Changes Following Manual Therapy in Resting State Functional Connectivity As Measured By Magnetic Resonance Imaging (fMRI) In Subjects With Induced Low Back Pain', *J Manipulative Physiol Ther* **37**(9), 614–627.

27. Ghez, C. & Krakauer, J. (2000), The Organization of Movement, *in* 'Principles of neural science', Vol. 4, pp. 653–867.

28. Haavik, H. (2014), *The reality check*, 1st editio edn, Haavik Research.

29. Haavik, H. & Murphy, B. (2012), 'The role of spinal manipulation in addressing disordered sensorimotor integration and altered motor control', *Journal of Electromyography and Kinesiology* **22**(5), 768–776.

30. Haavik, H., Niazi, I. K., Jochumsen, M., Sherwin, D., Flavel, S. & Türker, K. S. (2017), 'Impact of spinal manipulation on cortical drive to upper and lower limb muscles', *Brain Sciences* **7**(1), 1–15.

31. Haavik, H., Özyurt, M. G., Niazi, I. K., Holt, K., Nedergaard, R. W., Yilmaz, G. & Türker, K. S. (2018), 'Chiropractic manipulation increases maximal bite force in healthy individuals', *Brain Sciences* **8**(5), 1–9.

32. Hald, D. H. (2017), 'Generative Temporal Modelling of Neuroimaging – Decomposition and Nonparametric Testing Ditte Høvenhoff Hald'.

33. Hassan, M. & Wendling, F. (2018), 'Electroencephalography source connectivity : toward high time / space resolution brain networks', *IEEE Signal Processing Society* **35**(3), 1–25.

34. Hatz, F., Hardmeier, M., Bousleiman, H., Rüegg, S., Schindler, C. & Fuhr, P. (2015), 'Reliability of fully automated versus visually controlled pre- and post-processing of resting-state EEG', *Clinical Neurophysiology* **126**(2), 268–274.

35. HEBA SOFFAR (2018), 'The function of the spinal cord in the central nervous system'.
URL: *https://bit.ly/2EDpLmH*

36. Hennerici, M. G., Kern, R. & Binder, K. S. J. (2012), *Stroke*, 1 edn, Oxford University Press.

37. Holt, K., Niazi, I. K., Nedergaard, R. W., Duehr, J., Amjad, I., Shafique, M., Anwar, M. N., Ndetan, H., Turker, K. S. & Haavik, H. (2019), 'The effects of a single session of chiropractic care on strength, cortical drive, and spinal excitability in stroke patients', *Scientific Reports* **9**(1), 2673.

38. Horowitz, S. (2007), 'Evidence-based applications for chiropractic.', *Alternative & Complementary Therapies* **13**(5), 248–253.

39. Huang, G. & Zhang, Z. (2017), 'Improving sensitivity of cluster-based permutation test for EEG/MEG data', *International IEEE/EMBS Conference on Neural Engineering, NER* pp. 9–12.

40. Im, C.-H. (2018), *Biological and Medical Physics, Biomedical Engineering Computational EEG Analysis Methods and Applications*, Springer.

41. Islam, M. K., Rastegarnia, A. & Yang, Z. (2016), 'Les méthodes de détection et de rejet d'artefact de l'EEG de scalp : revue de littérature', *Neurophysiologie Clinique* **46**(4-5), 287–305.

42. Jin, S. H., Lin, P., Auh, S. & Hallett, M. (2011), 'Abnormal functional connectivity in focal hand dystonia: Mutual information analysis in EEG', *Movement Disorders* **26**(7), 1274–1281.

43. Johnson, C. (2013), 'Abstracts of the Scientific Sessions from the WFC'S 12th Biennial Congress Proceedings, Durban, South Africa, April 10-13, 2013', *Journal of Chiropractic Medicine* **12**(2), 92–142.

44. Kabbara, A., El Falou, W., Khalil, M., Wendling, F. & Hassan, M. (2017), 'The dynamic functional core network of the human brain at rest', *Scientific reports* **7**(1), 2936.

45. Karafin, M. S., Chen, G., Wandersee, N., Hubler, C., Brandow, A. M., Simpson, P., Li, S. J. & Field, J. J. (2016), 'Daily pain is associated with alterations in functional connectivity of the brain on fMRI in adults with sickle cell disease', *Blood* **128**(22), 1–13.

46. Khlebopros, A. (2015), 'Chiropractic care', *Alternative medicine* **1**(June), 58–60.
URL: *https://bit.ly/2rLIHXZ*

47. Klein, A. & Tourville, J. (2012), '101 Labeled Brain Images and a Consistent Human Cortical Labeling Protocol', *Frontiers in Neuroscience* **6**(DEC), 1–12.

48. Kolb, B., Mychasiuk, R., Muhammad, A., Li, Y., Frost, D. O. & Gibb, R. (2012), 'Experience and the developing prefrontal cortex', *Proceedings of the National Academy of Sciences* **109**(Supplement_2), 17186–17193.

49. Lai, M., Demuru, M., Hillebrand, A. & Fraschini, M. (2018), 'A comparison between scalp- and source-reconstructed EEG networks', *Scientific Reports* **8**(1), 1–8.

50. Langhorne, P., Bernhardt, J. & Kwakkel, G. (2011), 'Stroke rehabilitation', *The Lancet* **377**(9778), 1693–1702.

51. Lee, K. B., Yeom, J. W., Kim, K. H., Hwang, B. Y., Kim, K. J., Lim, S. H., Kim, Y. D., Chang, W. N. & Kim, Y. R. (2015), 'Six-month functional recovery of stroke patients', *International Journal of Rehabilitation Research* **38**(2), 173–180.

52. Legg, P., Rosin, P., Marshall, D. & Morgan, J. (2007), 'Improving Accuracy and Efficiency of Registration by Mutual Information using Sturges' Histogram Rule', *Proceedings of Medical Image Understanding and Analysis* pp. 26–30.

53. Lelic, D., Niazi, I. K., Holt, K., Jochumsen, M., Dremstrup, K., Yielder, P., Murphy, B., Drewes, A. M. & Haavik, H. (2016), 'Manipulation of dysfunctional spinal joints affects sensorimotor integration in the prefrontal cortex: A brain source localization study', *Neural Plasticity* .

54. Li, S., Zhou, M., Yu, B., Ma, Z., Chen, S., Gong, Q., He, L., Huang, X., Lui, S., Wang, X., Zhou, D. & He, C. (2014), 'Altered Defau lt Mode and Affective Network Connectivity in Stroke Patients with and without Dysphagia', *Journal of Rehabilitation Medicine* **46**(2), 126–131.

55. Lin, G. G.-h. & Scott, J. G. (2012), 'Modeling skull electrical properties', *Ann Biomed Eng.* **100**(2), 130–134.

56. Liu, J., Qin, W., Zhang, J., Zhang, X. & Yu, C. (2015), 'Enhanced Interhemispheric Functional Connectivity Compensates for Anatomical Connection Damages in Subcortical Stroke', *Stroke* **46**(4), 1045–1051.

57. Liu, Q., Ganzetti, M., Wenderoth, N. & Mantini, D. (2018), 'Detecting Large-Scale Brain Networks Using EEG: Impact of Electrode Density, Head Modeling and Source Localization', *Frontiers in Neuroinformatics* **12**(March), 1–11.

58. Lystad, R. P. & Pollard, H. (2009), 'Functional neuroimaging: a brief overview and feasibility for use in chiropractic research.', *The Journal of the Canadian Chiropractic Association* **53**(1), 59–72.
URL: *https://bit.ly/2QRmjrA*

59. Mang, C. S., Campbell, K. L., Ross, C. J. D. & Boyd, L. A. (2013), 'Perspective Promoting Neuroplasticity for Motor Rehabilitation After Stroke : Brain-Derived Neurotrophic Factor', *Physical Therapy* **93**(12), 1707–1716.

60. Manley, G. (2013), 'Public Access NIH Public Access', **71**(2), 233–236.

61. Manuscript, A. (2013), 'NIH Public Access', pp. 1–43.

62. Maris, E. & Oostenveld, R. (2007), 'Nonparametric statistical testing of EEG- and MEG-data', *Journal of Neuroscience Methods* **164**(1), 177–190.

63. Mayfield (2019), 'Stroke (brain attack)'.
URL: *https://mayfieldclinic.com/pe-stroke.htm*

64. Miller, M. B. (2013), Mathematics and Statistics for Financial Risk Management, *in* 'Journal of Mood Disorders', Vol. 3, John Wiley & Sons, Incorporated, chapter 10, p. 90.
URL: *http://www.scopemed.org/fulltextpdf.php?mno=39197*

65. Ming, D., Sun, C., Yang, F., Wang, C., Du, J., Wang, Z. & Zhang, Y. (2018), 'Mutual Information-Based Brain Network Analysis in Post-stroke Patients With Different Levels of Depression', *Frontiers in Human Neuroscience* **12**(July), 1–10.

66. Mir, M. A., Al-Baradie, R. S. & Alhussainawi, M. D. (2014), Pathophysiology of Strokes, *in* 'Recent Advances in Stroke Therapeutics', Nova Science Publishers, chapter 2, pp. 1–54.

67. Morgan, W. E. (2014), 'Manipulation Activates Muscles of the Core'.
URL: *https://bit.ly/2Bw21N8*

68. Morimoto, T., Inoue, T., Masuda, Y. & Nagashima, T. (1989), 'Sensory components facilitating jaw-closing muscle activities in the rabbit', *Experimental Brain Research* **76**(2), 424–440.

69. Mullen, T. R., Kothe, C. A. E., Chi, M., Ojeda, A., Kerth, T., Makeig, S. & Cauwenberghs, G. (2015), 'Real-time Neuroimaging and Cognitive Monitoring Using Wearable Dry EEG Tzyy-Ping Jung [Fellow, IEEE], and SCCN, INC, UCSD HHS Public Access', *IEEE Trans Biomed Eng* **62**(11), 2553–2567.

70. Newson, J. J. & Thiagarajan, T. C. (2019), 'EEG Frequency Bands in Psychiatric Disorders: A Review of Resting State Studies', *Frontiers in Human Neuroscience* **12**(January), 1–24.

71. Ni, Z. & Chen, R. (2012), *Cortical Connectivity——Brain Stimulation for Assessing and Modulating Cortical Connectivity and Function.*

72. Niazi, I. K., Türker, K. S., Flavel, S., Kinget, M., Duehr, J. & Haavik, H. (2015), 'Changes in H-reflex and V-waves following spinal manipulation', *Experimental Brain Research* **233**(4), 1165–1173.

73. O'Donnell, M. J., Diener, H. C., Sacco, R. L., Panju, A. A., Vinisko, R. & Yusuf, S. (2013), 'Chronic pain syndromes after ischemic stroke: PRoFESS trial', *Stroke* **44**(5), 1238–1243.

74. Ovbiagele, B. & Nguyen-Huynh, M. N. (2011), 'Stroke Epidemiology: Advancing Our Understanding of Disease Mechanism and Therapy', *Neurotherapeutics* **8**(3), 319–329.

75. Palmgren, P. J., Sandström, P. J., Lundqvist, F. J. & Heikkilä, H. (2006), 'Improvement after chiropractic care in cervicocephalic kinesthetic sensibility and subjective pain intensity in patients with nontraumatic chronic neck pain', *Journal of Manipulative and Physiological Therapeutics* **29**(2), 100–106.

76. Pascual-Marqui, R. D. (2002), 'Standardized low-resolution brain electromagnetic tomography (sLORETA): technical details.', *Methods and findings in experimental and clinical pharmacology* **24 Suppl D**, 5–12.

77. Pedroni, A., Bahreini, A. & Langer, N. (2018), 'AUTOMAGIC : Standardized Preprocessing of Big EEG Data', *bioRxiv* pp. 0–41.

78. Peterson, C. K., Bolton, J. & Humphreys, B. K. (2012), 'Predictors of improvement in patients with acute and chronic low back pain undergoing chiropractic treatment', *Journal of Manipulative and Physiological Therapeutics* **35**(7), 525–533.

79. Pickar, J. G. (2002), 'Neurophysiological effects of spinal manipulation', *Spine Journal* **2**(5), 357–371.

80. Pickar, J. G. & Kang, Y. M. (2006), 'Paraspinal muscle spindle responses to the duration of a spinal manipulation under force control', *Journal of Manipulative and Physiological Therapeutics* **29**(1), 22–31.

81. Preston, A. R. & Eichenbaum, H. (2013), 'Interplay of hippocampus and prefrontal cortex in memory', *Current Biology* **23**(17), 1–21.

82. Puig, J., Blasco, G., Alberich-Bayarri, A., Schlaug, G., Deco, G., Biarnes, C., Navas-Martí, M., Rivero, M., Gich, J., Figueras, J., Torres, C., Daunis-I-Estadella, P., Oramas-Requejo, C. L., Serena, J., Stinear, C. M., Kuceyeski, A., Soriano-Mas, C., Thomalla, G., Essig, M., Figley, C. R., Menon, B., Demchuk, A., Nael, K., Wintermark, M., Liebeskind, D. S. & Pedraza, S. (2018), 'Resting-State Functional Connectivity Magnetic Resonance Imaging and Outcome After Acute Stroke', *Stroke* **49**(10), 2353–2360.

83. Ramanand, P., Bruce, M. C. & Bruce, E. N. (2011), 'NIH Public Access', *Sleep (Rochester)* **27**(4), 274–284.

84. Robert F. Schmidt & Gerald F. Gebhart (2013), *Encyclopedia of Pain*, second edi edn, Springer.

85. Rosenblum, M., Pikovsky, A., Kurths, J., Schäfer, C. & Tass, P. A. (2001), 'Chapter 9 Phase synchronization: From theory to data analysis', *Handbook of Biological Physics* **4**(C), 279–321.

86. Rosjat, N., Abdollahi, R., Daun-Gruhn, S., Wang, B., Popovych, S., Liu, L., Grefkes, C., Viswanathan, S., Tóth, T. & Fink, G. (2016), 'EP 111. Phase-locking analysis of EEG-data in movement related tasks reveals functional network of synchronous activity', *Clinical Neurophysiology* **127**(9), e287–e288.

87. Roulston, M. S. (1999), 'Estimating the errors on measured entropy and mutual information', *Physica D: Nonlinear Phenomena* **125**(3-4), 285–294.

88. Rutkove, S. B. (2007), 'Introduction to volume conduction', *The Clinical Neurophysiology Primer* **C**, 43–53.

89. Sakkalis, V., Giurcaneacu, C., Xanthopoulos, P., Zervakis, M., Tsiaras, V., Yang, Y. & Micheloyannis, S. (2006), 'Assessment of linear and non-linear EEG synchronization measures for evaluating mild epileptic signal patterns', *Proc. of ITAB* **13**(4), 26–28.

90. Salehi A, Hashemi N, Imanieh MH, Saber M., Salehi, A., Hashemi, N., Imanieh, M. H. & Saber, M. (2015), 'Chiropractic: Is it Efficient in Treatment of Diseases? Review of Systematic Reviews.', *International journal of community based nursing and midwifery* **3**(4), 244–254.

91. Sazonov, A. V., Ho, C. K., Bergmans, J. W. M., Arends, J. B. A. M., Griep, P. A. M., Verbitskiy, E. A., Cluitmans, P. J. M. & Boon, P. A. J. M. (2009), 'An investigation of the phase locking index for measuring of interdependency of cortical source signals recorded in the EEG', *Biological Cybernetics* **100**(2), 129–146.

92. Sell, R., Rothenberg, M. A. & Chapman, C. (2012), Dictionary of Medical Terms, *in* R. Sell, M. A. Rothenberg & C. Chapman, eds, 'Dictionary of Medical Terms', sixth edit edn, Barrons Educational Series (July 2018), chapter S, pp. 516–555.

93. Seraj, E. (2018), 'Cerebral Synchrony Assessment: A General Review on Cerebral Signals' Synchronization Estimation Concepts and Methods'.

94. Siuly, S., Li, Y. & Yanchun Zhang (2016), *EEG Signal Analysis and Classification Techniques and Applications*, Springer.

95. Smith, V., Mitchell, D. J. & Duncan, J. (2018*a*), 'Role of the default mode network in cognitive transitions', *Cerebral Cortex* **28**(10), 3685–3696.

96. Smith, V., Mitchell, D. J. & Duncan, J. (2018*b*), 'Role of the Default Mode Network in Cognitive Transitions', (October), 3685–3696.

97. Stam, C. J., Nolte, G. & Daffertshofer, A. (2007), 'Phase lag index: Assessment of functional connectivity from multi channel EEG and MEG with diminished bias from common sources', *Human Brain Mapping* **28**(11), 1178–1193.

98. Summary, E. (2000), 'Brain Plasticity and Stroke Rehabilitation', **2343**(20), 1507–1512.

99. Sung, P. S., Kang, Y. M. & Pickar, J. G. (2005), 'Effect of spinal manipulation duration on low threshold mechanoreceptors in lumbar paraspinal muscles: A preliminary report', *Spine* **30**(1), 115–122.

100. Tadel, F., Baillet, S., Mosher, J. C., Pantazis, D. & Leahy, R. M. (2011), 'Brainstorm: A user-friendly application for MEG/EEG analysis', *Computational Intelligence and Neuroscience* **2011**.

101. Takeuchi, N. & Izumi, S. I. (2012), 'Maladaptive plasticity for motor recovery after stroke: Mechanisms and approaches', *Neural Plasticity* .

102. Taub, E., Uswatte, G. & Elbert, T. (2002), 'New treatments in neurorehabiliation founded on basic research', *Nature Reviews Neuroscience* **3**(3), 228–236.

103. Taylor, H. H., Holt, K. & MURPHY, B. (2010), 'Exploring the neuromodulatory effects of the vertebral subluxation and chiropractic care', *Chiropr J Aust* **40**(1), 37–44.
URL: *https://chiro.org/research/FULL/Exploring_the_Neuromodulatory_Effects.pdf*

104. Thompson, C. K. (2000), 'Neuroplasticity: Evidence from aphasia', *Journal of Communication Disorders* **33**(4), 357–366.

105. Treister, A. K., Hatch, M. N., Cramer, S. C. & Chang, E. Y. (2017), 'Demystifying Poststroke Pain: From Etiology to Treatment', *PM and R* **9**(1), 63–75.

106. Van Den Heuvel, M. P. & Pol, H. E. (2011), 'Exploring the brain network: A review on resting-state fMRI functional connectivity', *Psiquiatria Biologica* **18**(1), 28–41.

107. Vila-Chã, C., Falla, D., Correia, M. V. & Farina, D. (2012), 'Changes in H reflex and V wave following short-term endurance and strength training', *Journal of Applied Physiology* **112**(1), 54–63.

108. Wang, T., Bebbington, M. & Harte, D. (2010), 'A comparative study of coherence, mutual information and cross-intensity models', *Int J Info Sys Sci* **6**(1), 49–60.
URL: *https://bit.ly/2LqKoTC*

109. Wang, Z. J., Lee, P. W. H. & McKeown, M. J. (2009), 'A novel segmentation, mutual information network framework for EEG analysis of motor tasks', *BioMedical Engineering Online* **8**, 1–19.

110. Ward, A. M., Schultz, A. P., Huijbers, W., van Dijk, K. R., Hedden, T. & Sperling, R. A. (2013), 'Public Access NIH Public Access', **185**(2), 974–981.

111. Warraich, Z. & Kleim, J. A. (2010), 'Neural plasticity: The biological substrate for neurorehabilitation', *PM and R* **2**(12 SUPPL), S208–S219.

112. Westlake, K. P. & Nagarajan, S. S. (2011), 'Functional Connectivity in Relation to Motor Performance and Recovery After Stroke', *Frontiers in Systems Neuroscience* **5**(March), 1–12.

113. Wu, J., Quinlan, E. B., Dodakian, L., McKenzie, A., Kathuria, N., Zhou, R. J., Augsburger, R., See, J., Le, V. H., Srinivasan, R. & Cramer, S. C. (2015), 'Connectivity measures are robust biomarkers of cortical function and plasticity after stroke', *Brain* **138**(8), 2359–2369.

114. Zeiler, S. R. & Krakauer, J. W. (2013), 'The interaction between training and plasticity in the poststroke brain', *Current Opinion in Neurology* **26**(6), 609–616.

115. Zhou, Y., Dougherty, J. H., Hubner, K. F., Bai, B., Cannon, R. L. & Hutson, R. K. (2008), 'Abnormal connectivity in the posterior cingulate and hippocampus in early Alzheimer ' s disease and mild cognitive impairment', **4**, 265–270.

116. Zomet, A., Rav-Acha, A. & Peleg, S. (2001), 'Robust Super-Resolution*', pp. 645–650.

A | Brain region labeling

Table A.1: Brain region labels with abbreviation - Part 1. Whole brain connectivity includes all the listed regions. DMN connectivity only includes regions marked with **(DMN)** in the abbreviation

	Brain region	**Shortening**
1	L Frontal Pole	L FP
2	R Frontal Pole	R FP
3	L Superior Frontal Gyrus	L SFG
4	R Superior Frontal Gyrus	R SFG
5	L Rostral Middle Frontal Gyrus	L RMFG
6	R Rostral Middle Frontal Gyrus	R RMFG
7	L Medial Orbitofrontal	L MOF **(DMN)**
8	R Medial Orbitofrontal	R MOF **(DMN)**
9	L Lateral Orbitofrontal	L LOF **(DMN)**
10	R Lateral Orbitofrontal	R LOF **(DMN)**
11	L Pars Orbitalis	L POT
12	R Pars Orbitalis	R POT
13	L Pars Triangularis	L PSG
14	R Pars Triangularis	R PSG
15	L Pars Opercularis	L POC
16	R Pars Opercularis	R POC
17	L Caudal Middle Frontal Gyrus	L CMFG
18	R Caudal Middle Frontal Gyrus	R CMFG
19	L Precentral	L PreC
20	R Precentral	R PreC
21	L Postcentral	L PostC
22	R Postcentral	R PostC
23	L Paracentral	L ParaC
24	R Paracentral	R ParaC
25	L Superior Temporal gyrus	L STG
26	R Superior Temporal gyrus	R STG
27	L Transverse Temporal	L TT
28	R Transverse Temporal	R TT
29	L Middle Temporal Gyrus	L MTG
30	R Middle Temporal Gyrus	R MTG
31	L Inferior Temporal Gyrus	L ITG
32	R Inferior Temporal Gyrus	R ITG

Table A.2: Brain region labels with abbreviation - Part 2. Whole brain connectivity includes all the listed regions. DMN connectivity only includes regions marked with **(DMN)** in the abbreviation

	Brain region	**Shortening**
33	L Fusiform	L Fus
34	R Fusiform	R Fus
35	L Temporal pole	L TP
36	R Temporal pole	R TP
37	L Insula	L Ins
38	R Insula	R Ins
39	L Entorhinal	L Ent
40	R Entorhinal	R Ent
41	L Parahippocampal	L ParaH **(DMN)**
42	R Parahippocampal	R ParaH **(DMN)**
43	L Lingual	L Lin
44	R Lingual	R Lin
45	L Isthmus Cingulate Cortex	L ICC **(DMN)**
46	R Isthmus Cingulate Cortex	R ICC **(DMN)**
47	L Precuneus	L Precun **(DMN)**
48	R Precuneus	R Precun **(DMN)**
49	L Posterior Cingulate Cortex	L PCC **(DMN)**
50	R Posterior Cingulate Cortex	R PCC **(DMN)**
51	L Cuneus	L Cun
52	R Cuneus	R Cun
53	L Lateral Occipital Gyrus	L LOG
54	R Lateral Occipital Gyrus	R LOG
55	L Superior Parietal Lobule	L SPL
56	R Superior Parietal Lobule	R SPL
57	L Inferior Parietal Lobule	L IPL
58	R Inferior Parietal Lobule	R IPL
59	L Bank Of The Superior Temporal Sulcus	L BTSTS
60	R Bank Of The Superior Temporal Sulcus	R BTSTS
61	L Caudal Anterior Cingulate	L CAC
62	R Caudal Anterior Cingulate	R CAC
63	L Pericalcarine	L Peri
64	R Pericalcarine	R Peri
65	L Rostral Anterior Cingulate Cortex	L RACC **(DMN)**
66	R Rostral Anterior Cingulate Cortex	R RACC **(DMN)**
67	L Supramarginal Gyrus	L SMG
68	R Supramarginal Gyrus	R SMG

B | Adjacency matrices with tended and significant clusters

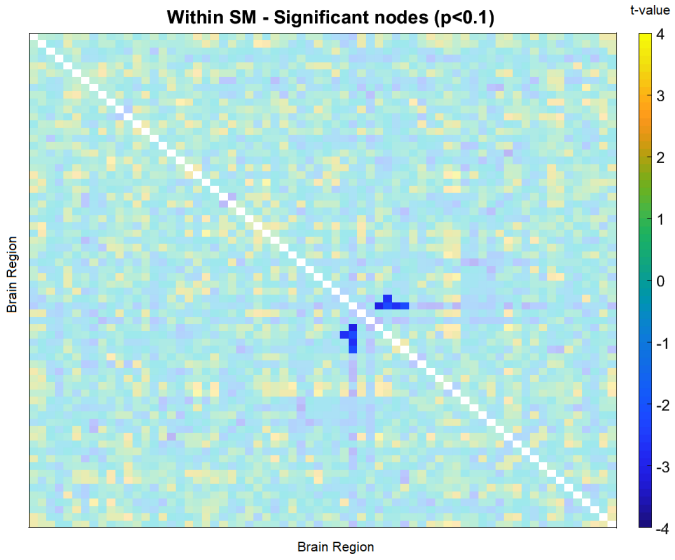

Figure B.1: Significant clusters in the adjacency matrices from whole brain Alpha of comparison within SM session, illustrated by their t-values. Negative t-values are reflecting a decrease in connectivity while positive t-values are reflecting an increase. Labels can be found in appendix B

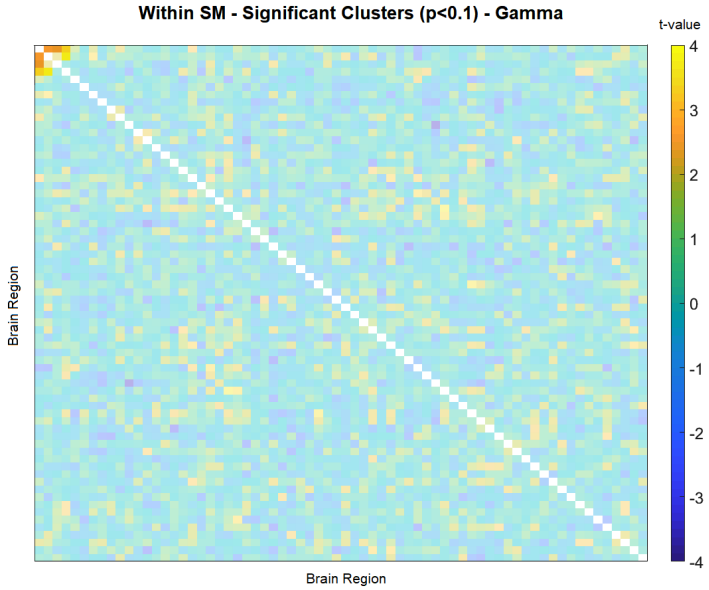

Figure B.2: Significant clusters in the adjacency matrices from whole brain Gamma of comparison within SM session, illustrated by their t-values. Negative t-values are reflecting a decrease in connectivity while positive t-values are reflecting an increase. Labels can be found in appendix B

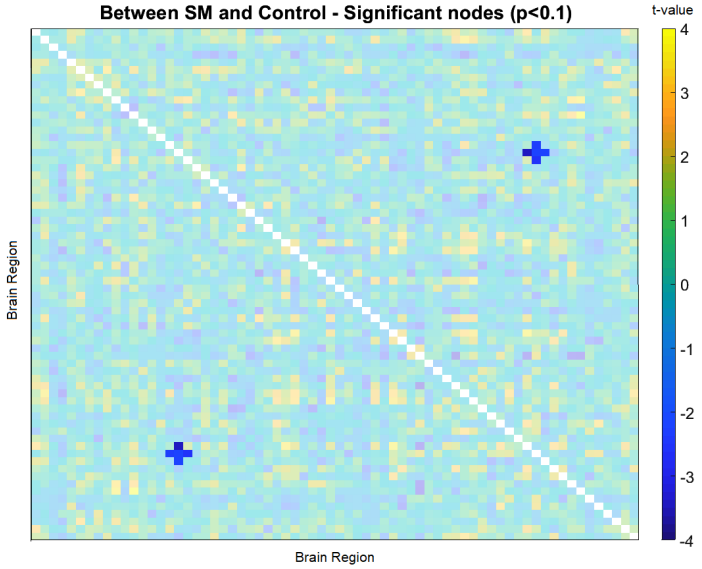

Figure B.3: Significant clusters in the adjacency matrices from whole brain Alpha of comparison between SM vs. Ctrl, illustrated by their t-values. Negative t-values are reflecting a decrease in connectivity while positive t-values are reflecting an increase. Labels can be found in appendix B

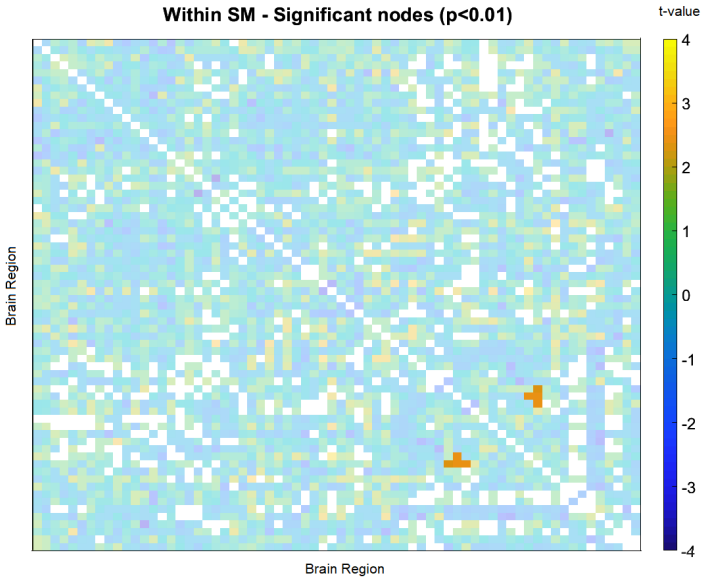

Figure B.4: Significant clusters in the adjacency matrices illustrated by their t-values. Negative t-values are reflecting a decrease in connectivity while positive t-values are reflecting an increase. Labels can be found in appendix B

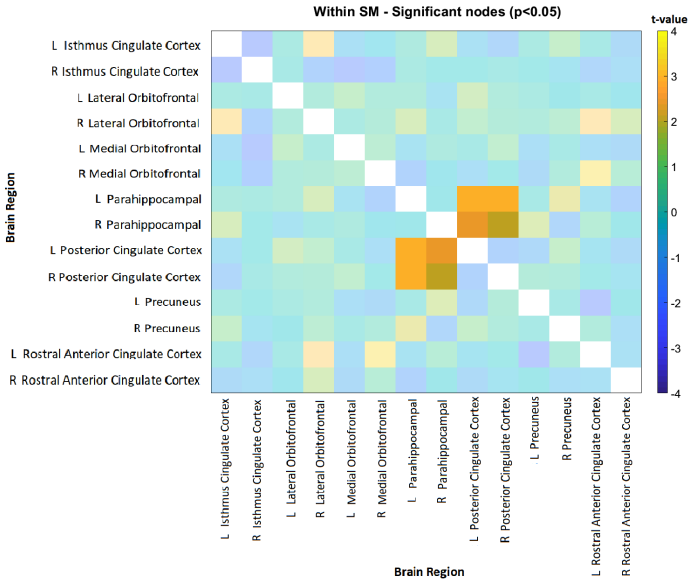

Figure B.5: Significant clusters in the adjacency matrices from DMN Alpha of comparison within the SM session, illustrated by their t-values. Negative t-values are reflecting a decrease in connectivity while positive t-values are reflecting an increase. Labels can be found in appendix B

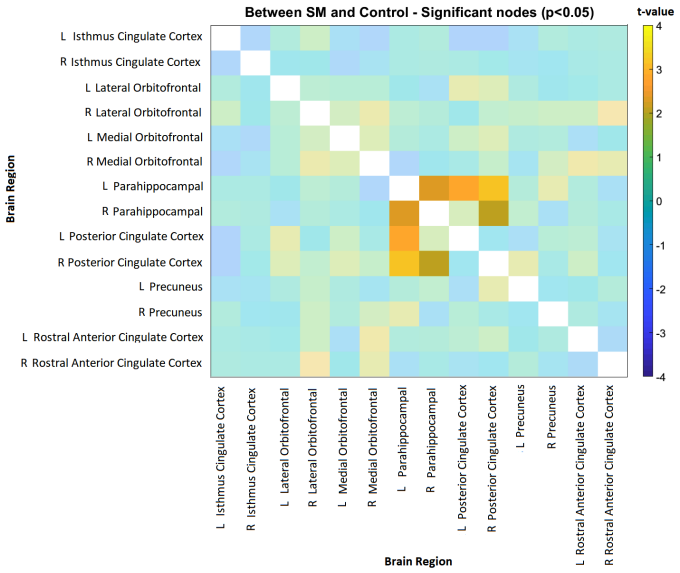

Figure B.6: Significant clusters in the adjacency matrices from DMN Alpha of comparison between SM vs. Ctrl, illustrated by their t-values. Negative t-values are reflecting a decrease in connectivity while positive t-values are reflecting an increase. Labels can be found in appendix B

C | DMN MI result table

Table C.1: DMN comparison for MI. Positive (+) and negative (-) cluster count are shown, with t-value and p-values in case of any significant clusters were present

p<0.05			If significant			If significant	
		+ clusters	**t-value**	**p-value**	**- clusters**	**t-value**	**p-value**
Alpha	SM vs. Ctrl	114	-	-	134	-	-
	SM	130	-	-	98	-	-
	Ctrl	136	-	-	98	-	-
Beta	SM vs. Ctrl	92	-	-	108	-	-
	SM	110	-	-	116	-	-
	Ctrl	94	-	-	84	-	-
Gamma	SM vs. Ctrl	94	-	-	94	-	-
	SM	120	-	-	90	-	-
	Ctrl	94	-	-	110	-	-

D | Signal variation

Table D.1: Possible signal range within the dataset

	Alpha	Beta	Gamma
Max.	9.65 e-09	7.91 e-09	2.59 e-09
Min.	-9.28 e-09	-8.01 e-09	-2.58 e-09

E | Desikan-Killarney atlas brain regions

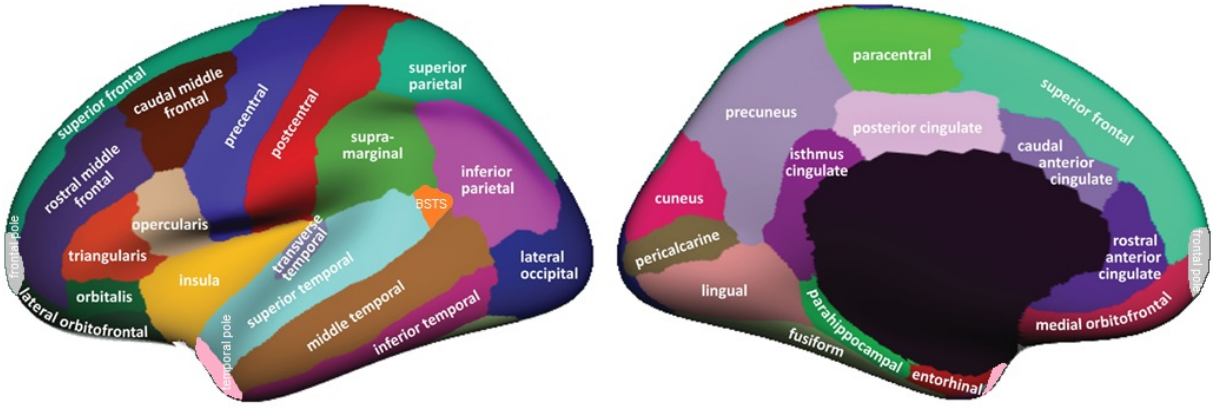

Figure E.1: Illustration of the organization of brain regions of the Desikan-Killarney atlas [Klein & Tourville (2012)]